Ecological Engineering 179 (2022) 106621

Contents lists available at ScienceDirect

Ecological Engineering

journal homepage: www.elsevier.com/locate/ecoleng

DRAM: A three-dimensional analytical model for the mobilisation of root reinforcement in direct shear conditions

G.J. Meijer [a,*], J.A. Knappett [b], A.G. Bengough [b], D.J. Bull [c], T. Liang [d], D. Muir Wood [b]

[a] Department of Architecture and Civil Engineering, University of Bath, Bath BA2 7AY, UK
[b] School of Science and Engineering University of Dundee, Dundee DD1 4HN, UK
[c] Faculty of Engineering and Physical Sciences, University of Southampton, Southampton SO17 1BJ, UK
[d] Center for Hypergravity Experimental and Interdisciplinary Research, College of Civil Engineering and Architecture, Zhejiang University, Hangzhou, Zhejiang 310058, China

ARTICLE INFO

Keywords:
Root reinforcement
Direct shear
Landslides
Analytical modelling
Vegetation

ABSTRACT

Roots can stabilise slopes against shallow landslides by mobilising their mechanical strength. Existing analytical models are highly simplified and typically focus on the ultimate limit state only, thus providing little insight into the underlying mechanism of reinforcement mobilisation. A new analytical model ('DRAM') was therefore developed to predict mechanical root reinforcement as a function of direct shear displacements. This model accounts for elasto-plastic root behaviour, three-dimensional root orientations, root failure through breakage or slippage, and a dynamically changing shear zone thickness.

Comparison to two independent experimental direct shear data sets showed that the model was able to accurately predict the gradual mobilisation of root strength, the magnitude of peak root reinforcement, as well as the presence of significant root reinforcement at large shear displacements, associated with a relatively large quantity of roots slipping out of the surrounding soil.

Because the newly developed model more closely resembles the underlying physics of the mobilisation of root reinforcement in direct shear while still being easy to use, it will be a useful tool for the engineering industry, in terms of quantifying root reinforcement distribution for limit analyses at the ultimate limit state, as well as for directing future research into the drivers of mechanical root reinforcement.

1. Introduction

The modelling of the mechanical reinforcement of soil by plant roots is challenging due to the complicated interaction between soil and roots. Root reinforcement is typically studied in the context of slope stability, where the parameter of interest is the peak shear strength of the rooted soil (Coppin and Richards, 1990; Stokes et al., 2009). Various analytical models have been developed to predict this peak strength at the ultimate limit state, which are discussed in the following paragraphs.

The most well-known root reinforcement model has become known as the Wu/Waldron Model ('WWM', Waldron, 1977; Wu et al., 1979), expressing the increase in soil shear strength by an increase in soil cohesion, c_r. They hypothesised roots reinforce the soil by two mechanisms:

1. The component of root tensile stress in the direction of shearing will directly add to the shear resistance of the soil–root composite;
2. The component of root tensile stress normal to the shear plane will result in additional soil confinement pressure on the shear plane, resulting in additional soil shear resistance.

In equation form, summing over all root sizes i:

$$c_r = \sum_i \phi_r t_r (sin\beta + cos\beta tan\phi') \quad (1)$$

where t_r is the tensile stress in roots of size i [FL^{-2}],[1] ϕ_r the root area

* Corresponding author.
E-mail address: gjm36@bath.ac.uk (G.J. Meijer).

[1] All parameters in this manuscript (in square brackets) are expressed in general dimensions unless otherwise specified: [F] for units of force, [L] for units of length/diameter and [°] for units of angles. This allows the reader to use the unit system of their choice, as long as it is internally consistent. For example, if forces are expressed in Newtons and diameters in meters, it follows that stresses and stiffnesses [FL^{-2}] are given in units of Pascal (Newton per meter squared) etc.

https://doi.org/10.1016/j.ecoleng.2022.106621
Received 23 July 2021; Received in revised form 17 February 2022; Accepted 15 March 2022
Available online 25 March 2022

ratio of root size i [L^2L^{-2}], β the angle between the (displaced) root orientation and the normal to the shear zone [°], and ϕ' the soil angle of internal friction [°].

In practice, the WWM is only used when calculating the peak root reinforcement $c_{r,u}$, assuming (a) t_r is equal to the root tensile strength $t_{r,u}$, and (b) the bracketed term in Eq. (1) can be simplified as a constant, k', often assumed as $k' = 1.2$ (Wu et al., 1979). In this form, the WWM assumes all roots fail simultaneously in tension. This has often been cited as the main reason why the WWM has been found to significantly overestimate reinforcement, as in the real world roots will mobilise their strength progressively. Therefore an additional reduction factor k'' can be applied, for which a large range of values has been previously suggested based on experiments, ranging from $k'' = 0.2$ to $k'' = 1.0$ (Wu and Watson, 1998; Operstein and Frydman, 2000; Comino et al., 2010; Preti, 2013; Meijer et al., 2018, among many others):

$$c_{r,u} = k' k'' \sum_i \phi_r t_{r,u} \tag{2}$$

Fibre bundle models ('FBM') have been used to incorporate progressive root failure (Pollen and Simon, 2005), typically defined in terms of a force-driven mechanism. In these models, the total tensile load in a bundle of roots is distributed among all intact roots. An important modelling choice is how to distribute the load between roots of different size and with different mechanical properties. Often root diameter d_r [L] is used, in which case the distribution in tensile force F in two unbroken roots ('i' and 'j') can be described by (Meijer, 2021):

$$\frac{F_i}{F_j} = \left(\frac{d_{r,i}}{d_{r,j}}\right)^{\beta_F} \tag{3}$$

where β_F is a (dimensionless) load sharing parameter. Once the tensile force exceeds the strength in a single root, it breaks and the load it carried is distributed over the remaining intact roots. Incrementally increasing the load until all roots have failed yields the maximum force the bundle can sustain, and thus the maximum root reinforcement $c_{r,u}$. Common choices of β_F are $\beta_F = 0$ (load is equally distributed over all roots, regardless of the diameter); $\beta_F = 1$ (load is split proportional to root diameters) and $\beta_F = 2$ (resulting in equal stresses in all roots) (see for example Comino et al., 2010; Thomas and Pollen-Bankhead, 2010; Mao et al., 2012), although more recently other load sharing mechanisms have been proposed (Ji et al., 2020; Meijer, 2021).

The great advantages of the WWM and FBMs described above are (a) their ease of use, and (b) the small number of input parameters (root quantities and biomechanical properties only). However, these models have significant drawbacks:

- They can only be used to capture the peak root reinforcement, $c_{r,u}$, and do not provide any information of associated shear deformations and 'stiffness' of the root reinforcement. Such displacements may be relevant when considering the stability of (root-reinforced) infrastructure embankments or cuttings with tight displacements tolerances (so-called 'serviceability limit state' problems, e.g. Briggs et al., 2016), or when identifying a limiting deformation of a slope that may be indicative of it approaching the ultimate limit state.
- Load sharing mechanisms are highly simplified, based on root properties only and assuming all roots are parallel. Thus other factors affecting sequential loading of roots, such as the influence of soil properties and especially the variation in root orientations, are ignored;
- They assume that, sooner or later, all roots will fail in tension. It is however often observed that roots may slip rather than break, for example on landslide scarps by Schmidt et al. (2001). Ignoring slippage may result in overestimation of root reinforcement.

Other existing root reinforcement models include a mechanism describing how reinforcement is mobilised as a function of displacements in the soil. One such model is the 'root bundle model' ('RBMw'), an alternative fibre bundle approach developed by Schwarz et al. (2013). This model assumes all roots elongate by the same amount u_r [L]. The root length L_r [L] may vary as a function of root diameter according to a power law. The strain in each root is assumed equal along the entire root length L_r, so $\varepsilon_r = u_r/L_r$, and roots are assumed linear elastic:

$$t_r = E_{r,e}\varepsilon_r = E_{r,e}\left(\frac{u_r}{L_r}\right) \tag{4}$$

where $E_{r,e}$ is the root elastic stiffness [FL^{-2}]. Some studies such as Dazio et al. (2018) use a secant stiffness rather than the Young's modulus. Schwarz et al. (2013) introduced a (dimensionless) breakage parameter f_b, defined as the probability that a root is still unbroken given the (normalised) displacement applied to the root (Δx^* [LL^{-1}]). Because of the assumed linear relations between tensile displacements, strains, forces and stresses, it can alternatively be expressed in terms of the tensile stress currently experienced by the root:

$$f_b = exp\left(-\left[\frac{\Delta x^*}{\lambda^*}\right]^{\kappa}\right) = exp\left(-\left[\frac{t_r}{\lambda}\right]^{\kappa}\right) \tag{5}$$

where κ [dimensionless] and λ [FL^{-2}] are the Weibull shape and scale parameter respectively. Note that λ is a scaled version of the (dimensionless) scale parameter λ^* used by Schwarz et al. (2013) due to the transformation from displacement to tensile stress. The 'average' root in the Weibull distribution must break when its tensile strength is exceeded. Using the mathematical expression for the mean of the Weibull distribution reveals that:

$$t_{r,u} = \lambda\Gamma\left(1 + \frac{1}{\kappa}\right) \tag{6}$$

where $\Gamma()$ is the gamma function. This shows that under the assumptions of the RBMw, the Weibull scale parameter λ (or alternatively, λ^*) cannot be independently chosen from the root strength and/or the assumed mobilisation mechanism, and that an alternative but equivalent expression for the breakage parameter f_b is:

$$f_b = exp\left(-\left[\Gamma\left(1 + \frac{1}{\kappa}\right)\frac{t_r}{t_{r,u}}\right]^{\kappa}\right) \tag{7}$$

As expcted, when κ approaches infinity, the breakage parameter f_b simplifies to:

$$f_b = \begin{cases} 1 & \text{when } t_r < t_{r,u} \\ 0 & \text{when } t_r > t_{r,u} \end{cases} \tag{8}$$

At a given displacement u_r, the current root reinforcement can be calculated by summing the contribution of all roots:

$$c_r = k' \sum \phi_r t_r f_b \tag{9}$$

And therefore the peak root reinforcement $c_{r,u}$ can be found by finding the maximum of c_r over the domain $0 \leq u_r \leq \infty$. The RBMw was originally developed for tensile condition such as root pullout along the crown of a landslide. To convert to direct shear conditions, Wu et al. (1979)'s orientation factor k' may be required as well as an additional assumption for how root elongation u_r relates to direct shear displacement u_s in the soil.

An alternative model, directly valid for direct shear conditions, was developed by Waldron (1977). Here, roots were assumed linear elastic (stiffness $E_{r,e}$), which, when the soil has not yet deformed,

perpendicularly cross a shear plane with constant thickness h [L]. Roots were assumed sufficiently long so that root slippage did not occur. With these assumptions, the root tensile stress t_r as a function of shear displacement u_s [L]:

$$t_r = \sqrt{\frac{4\tau_i E_{r,e} h}{d_r}}\sqrt{(sec\beta - 1)} \tag{10}$$

where τ_i is the root–soil interface shear resistance [FL^{-2}], and β is the angle between the displaced root and a vector normal to the shear plane [°]:

$$tan\beta = \frac{u_s}{h} \tag{11}$$

Roots break when the tensile stress t_r exceeds the tensile strength $t_{r,u}$. Calculated values for t_r were combined with Eq. (1) to acquire root reinforcements.

Waldron and Dakessian (1981) expanded Waldron's original model to include root slippage. Roots may slip rather than break when roots are relatively short and/or soil confinement is limited. This happens when the root tensile stress reaches a limiting slippage stress $t_{r,s}$ [FL^{-2}], at which point the tensile stress can increase no further and root ends will start to move ('slip') with increasing shear displacements instead:

$$t_{r,s} = \frac{2\tau_i L_r}{d_r} \tag{12}$$

Individual roots will slip rather than break when slippage stress $t_{r,s}$ is smaller than the tensile strength $t_{r,u}$.

The models by Waldron (1977) and Waldron and Dakessian (1981) provide a geometrically plausible mechanism for the mobilisation of root reinforcement in direct shear. They however have seldom been used in root reinforcement research and practice, and seem to have been mostly overlooked in favour of the much easier ultimate limit state approach building on the work of Wu et al. (1979).

In this paper, a new analytical model for mobilisation of root reinforcement in direct shear conditions is developed, extending the original methodology proposed by Waldron (1977) and Waldron and Dakessian (1981) by addressing three key model shortcomings:

- Root stress–strain behaviour. When considering the mobilisation of reinforcement, the root tensile stress–strain behaviour needs to be modelled accurately. Roots are often assumed linear elastic up the the point of failure (e.g. Waldron, 1977; Schwarz et al., 2013), while experimental evidence shows root stiffness is significantly reduced after yielding (Loades et al., 2013), suggesting elasto-plastic behaviour is more appropriate;
- Root orientations: Existing models assume that all roots cross the shear zone at a perpendicular angle (in the undeformed state). The effect of displaced orientations is normally accounted for through a single multiplication factor k'. In reality, (undeformed) root orientations may vary in position in three-dimensional space, which will strongly affect sequential mobilisation of roots and therefore peak root reinforcements;
- Shear zone thickness: Waldron-type models require an estimation for root angle β (Eq. (11)), which depends on the thickness of the shear zone (h, assumed constant) as well as shear displacement u_s. h has been reported to be large (80–250 mm) in field shear box tests on rooted soil (Abernethy and Rutherfurd, 2001; Burroughs and Thomas, 1977; Wu and Watson, 1998; Fan and Su, 2008), and was found to be larger in rooted or fibre-reinforced soil compared to fallow soils (Jewell and Wroth, 1987; Shewbridge and Sitar, 1989). Therefore some method for predicting how the shear zone thickness might increase as root reinforcement is mobilised is required.

This new model, referred to as the 'Dundee Root Analytical Model' ('DRAM'), provides a more mechanically rigorous model for the mobilisation of mechanical root reinforcement as a function of soil shear displacement based on the underlying physics of the problem. This model accounts for progressive root mobilisation, not only as a function of root diameter, but also as a function of root biomechanical properties, soil properties and, crucially, root orientations. The performance of the model will be compared to existing displacement-driven reinforcement models using two sets of experimental direct shear test data.

2. Methods: model description

The three new model components will be addressed in turn in the subsequent sections:

2.1. Root biomechanical behaviour

The behaviour of roots is not linear elastic in tension. The initial behaviour is relatively stiff up to a point of yielding, after which the tensile stiffness dramatically reduces (Loades et al., 2013). In the proposed model, this elasto-plastic root behaviour is therefore approximated using a bilinear relationship, see Fig. 1. Up to yield tensile stress $t_{r,y}$ [FL^{-2}] the root behaves linear elastically with elastic stiffness $E_{r,e}$ [FL^{-2}]:

$$E_{r,e} = \frac{t_{r,y}}{\varepsilon_{r,y}} \tag{13}$$

where $\varepsilon_{r,y}$ is the tensile strain at yielding [LL^{-1}]. After exceeding the yield stress, the stiffness is reduced to a (lower) linear stiffness $E_{r,p}$ representing the plastic tensile stiffness [FL^{-2}], up to the point where the tensile strength $t_{r,u}$ [FL^{-2}] is exceeded, at which point the root breaks:

$$E_{r,p} = \frac{t_{r,u} - t_{r,y}}{\varepsilon_{r,u} - \varepsilon_{r,y}} \tag{14}$$

where $\varepsilon_{r,u}$ is the root tensile strain at failure [LL^{-1}].

In tension tests, root tortuosity may cause an (apparent) reduction in the initial stiffness as roots straighten and stretch simultaneously. Tortuosity is driven by the geometry of the root rather than its biomechanical properties such as the Young's modulus. While it may be possible to (partially) account for tortuosity through careful adjustment

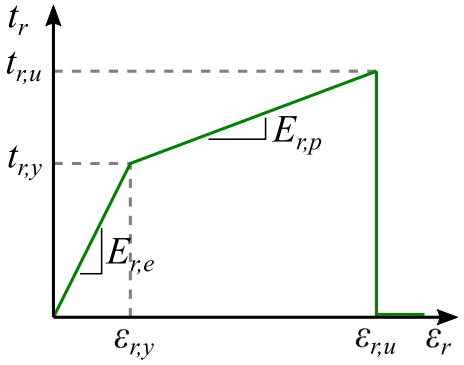

Fig. 1. Schematisation of root tensile stress (t_r) versus tensile strain (ε_r). The root behaviour is assumed linear elastic up to yielding ($\varepsilon_{r,y}$, $t_{r,y}$), followed by a reduced linear elasto-plastic stiffness $E_{r,p}$ up till the point of tensile failure ($\varepsilon_{r,u}$, $t_{r,u}$).

of root stiffness, all roots were assumed to be straight during development of the DRAM.

2.2. Extension of the WWM to three dimensions

Coordinates and angles are expressed in a right-handed coordinate system, orientated in such a way that x points in the direction of shear displacement u_s, and z is normal to the shear plane, pointing in the direction of the displacing soil block, see Fig. 2. h indicates the current thickness of the shear zone.

The orientation of undisplaced roots is described in spherical coordinates; azimuth α_0 (the angle between the x axis and the orientation of the root projected on the x-y plane) and elevation angle β_0 (angle between z-axis and root axis). The azimuth and elevation angles of the displaced root within the shear zone are indicated by α and β respectively. Transverse relative soil–root displacements are assumed to be zero, similar to assumptions by Waldron (1977) and Waldron and Dakessian (1981). This means each section of root always rotates by the same amount as the surrounding soil and can only move in the (rotated) root-axial direction.

Using spherical coordinates makes extending Eq. (1) to include three dimensions straightforward:

$$c_r = \sum_i \phi_r t_r (cos\alpha sin\beta + cos\beta tan\phi') \tag{15}$$

This shows that only the tangential component of root reinforcement is affected by the inclusion of three-dimensional root orientations.

The deformed orientation of roots within the shear zone can be found using trigonometry, see Fig. 2c:

$$cos\alpha = \frac{\xi_x}{\sqrt{\xi_x^2 + \xi_y^2}} \tag{16}$$

$$cos\beta = \frac{h}{\sqrt{\xi_x^2 + \xi_y^2 + h^2}} \tag{17}$$

$$sin\beta = \frac{\sqrt{\xi_x^2 + \xi_y^2}}{\sqrt{\xi_x^2 + \xi_y^2 + h^2}} \tag{18}$$

where:

$$\xi_x = h cos\alpha_0 tan\beta_0 + u_s \tag{19}$$

$$\xi_y = h sin\alpha_0 tan\beta_0 \tag{20}$$

2.3. Mobilisation of root tensile strength

Root tensile strength is progressively mobilised with increasing shear displacements. In this section, model formulations for the tensile stress in individual roots (t_r) are introduced. The following additional assumptions were made:

1. Roots behave like cable elements (i.e. bending and shear stiffnesses are both zero), and only reinforce in pure tension, not in compression, bending nor shear;
2. Undeformed roots are straight, unbranched prisms (with cross-sectional area A_r [L^2], circumference C_r [L] and length L_r [L]) that are not connected to other roots at either root end. Root properties may be different for each root. It is assumed that half of the root length is located below the shear plane, similar to the underlying assumption by Waldron and Dakessian (1981).

Roots may behave in four different ways. For each, the root tensile stress t_r within the shear zone has to be defined separately: (a) roots that are not in tension, (b) 'anchored' roots, i.e. roots that are sufficiently anchored in the surrounding soil so that the root ends do not slip, (c) slipping roots and (d) broken roots.

(a) Roots not in tension: The increase in the length of the (stretched) root (u_r, [L]) will change as a result of shear displacement (Fig. 3b):

$$u_r = \frac{h}{cos\beta} - \frac{h}{cos\beta_0} \tag{21}$$

When $u_r \leq 0$ (or alternatively, cos $\beta \geq$ cos β_0), the root does not increase in length and will therefore not be loaded in tension. In this case, the tensile stress in the root will be $t_r = 0$, i.e. it is assumed that roots cannot carry compressive stresses.

(b) Anchored roots: The tensile stress in the root will reduce with increasing distance from the shear zone because of transfer of stress through axial soil–root interface friction. When the root is sufficiently long, the root ends will not be loaded in tension and will not displace (Fig. 3b). This type of root behaviour is called 'anchored'.

It was assumed that the full soil–root interface friction τ_i is mobilised as soon as there is a finite relative soil–root displacement (i.e. rigid-perfectly plastic interface behaviour).

Assume for the moment that the root behaviour is linear elastic and root breakage is ignored. Within the shear zone, no interface friction is assumed to be present, so the root tensile stress in these 'anchored' roots ($t_{r,a}$, [FL^{-2}]) and the the corresponding tensile strain within the shear zone ($\varepsilon_{r,a} = t_{r,a}/E_{r,e}$) are constant. On either side of the shear zone interface friction is mobilised over a length L_e [L] until the tensile stress in the root has reduced to zero (Fig. 3c):

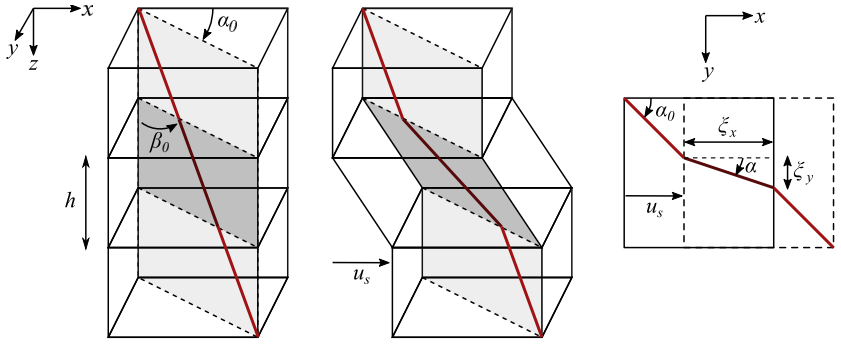

Fig. 2. Definition of root orientations in undisplaced soil (subplot a), and soil displaced by a shear displacement u_s and a shear zone thickness h (subplots b and c).

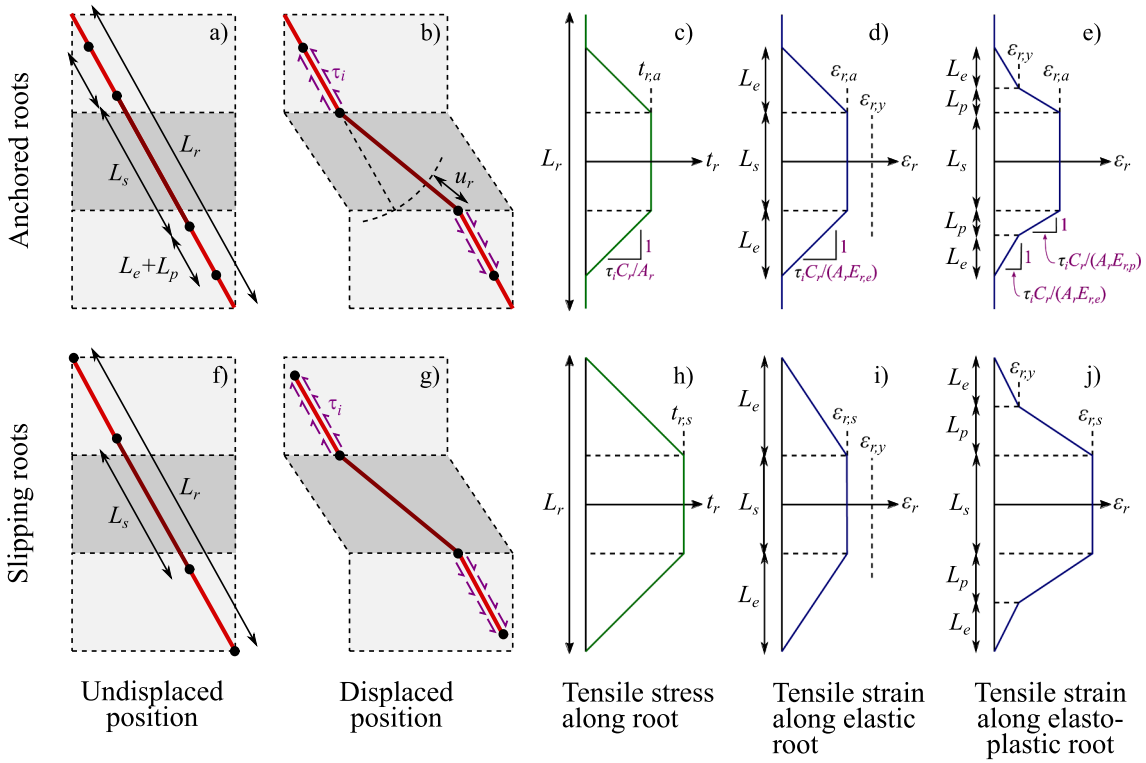

Fig. 3. Distribution of root displacements, tensile stresses and tensile strains (columns) along anchored or slipping roots (rows).

$$L_e = \frac{t_{r,a} A_r}{\tau_i C_r} \tag{22}$$

The (undisplaced) length of the section of root that ends up in the shear zone (L_s, [L]) is given by (Fig. 3a,b):

$$L_s = \frac{h}{cos\beta} \frac{1}{(1+\varepsilon_{r,a})} \tag{23}$$

The tensile stress distribution along the root is known (Fig. 3c), and because the root stress-strain behaviour is known, so is the tensile strain distribution along the root. Integrating this tensile strain along the root axis yields a second expression for the increase in root length (area under the curve in Fig. 3d):

$$u_r = \int_s \varepsilon_r \mathrm{d}s = (L_s + L_e)\varepsilon_{r,a} \tag{24}$$

where s is a coordinate along the root axis.

Both expressions for the total root elongation, one based on the geometry of the problem (Eq. (21)) and one based on tensile strains in the root (Eq. (24)) should be equal. After substitution of expressions, the tensile stress $t_{r,a}$ in the shear plane for anchored roots follows from the resulting cubic polynomial equation, for which analytical solutions exist:

Table 1
Polynomial coefficients for calculating stresses in anchored roots (Eq. (25)).

Coefficient	Elastic solution	Elasto-plastic solution
ξ_3	$\frac{A_r}{\tau_i C_r}\frac{1}{E_{r,e}^2}$	$\frac{A_r}{\tau_i C_r}\frac{1}{E_{r,p}^2}$
ξ_2	$\frac{A_r}{\tau_i C_r}\frac{1}{E_{r,e}}$	$\frac{A_r}{\tau_i C_r}\frac{1}{E_{r,p}}(1-3\zeta)$
ξ_1	$\frac{h}{cos\beta_0}\frac{1}{E_{r,e}}$	$\frac{h}{cos\beta_0}\frac{1}{E_{r,p}}+\zeta\frac{A_r}{\tau_i C_r}\left[\frac{t_{r,y}}{E_{r,p}}-2(1-\zeta)\right]$
ξ_0	$\frac{h}{cos\beta_0}-\frac{h}{cos\beta}$	$\frac{h}{cos\beta_0}-\frac{h}{cos\beta}+\zeta\left[\frac{A_r}{\tau_i C_r}t_{r,y}(1-\zeta)-\frac{h}{cos\beta_0}\right]$

$$\xi_3 t_{r,a}^3 + \xi_2 t_{r,a}^2 + \xi_1 t_{r,a} + \xi_0 = 0 \tag{25}$$

Expressions for ξ-coefficients can be found in Table 1. To simplify expressions, these solutions make use of an intermediate variable ζ:

$$\zeta = \frac{t_{r,y}}{E_{r,p}} - \frac{t_{r,y}}{E_{r,e}} \tag{26}$$

This approach is the same as that of Waldron (1977) with the key difference that they assumed $L_s = 0$ (i.e. to more simply calculate the root tensile stress profile along the root, they assumed the shear zone thickness was zero).

However, if the calculated (elastic) tensile stress $t_{r,a}$ exceeds the root tensile yield stress $t_{r,y}$, the root will behave plastically along part of the root length. In this case, the length over which root-soil interface friction is mobilised (on either side of the shear zone) consists of an elastic part (L_e) and plastic part (L_p [L]), see Fig. 3e:

$$L_e = \frac{t_{r,y} A_r}{\tau_i C_r} \tag{27}$$

$$L_p = \frac{(t_{r,a} - t_{r,y}) A_r}{\tau_i C_r} \tag{28}$$

The tensile strain in the root within the shear zone equals:

$$\varepsilon_{r,a} = \varepsilon_{r,y} + \frac{t_{r,a} - t_{r,y}}{E_{r,p}} \tag{29}$$

Integrating the root strain along the root axis results in another expression for the total root elongation (area underneath the curve in Fig. 3e):

$$u_r = \int_s \varepsilon_r \mathrm{d}s = (L_e + L_p)\varepsilon_{r,y} + (L_p + L_s)\varepsilon_{r,a} \tag{30}$$

Rewriting this system of equations again results in a cubic polynomial equation that can be solved to find $t_{r,a}$. Polynomial coefficients for the

elasto-plastic case are also given in Table 1.

Assuming the roots behave as 'anchored', the tensile stress in the shear zone $t_{r,a}$ can be found by first using the elastic solution, and if the calculated tensile stress exceeds the root yield stress, the elasto-plastic solution.

c) Slipping roots: Previously for 'anchored' roots, it was assumed that the roots were infinitely long. In reality, the tensile strength that can mobilise in the root may be limited by the root length along which root–soil interface friction may be mobilised. Once friction has mobilised along the full root length, the root tensile stress cannot increase any further and the root will 'slip' through the soil (Fig. 3g). When this happens, the corresponding limiting root tensile stress within the shear zone $t_{r,s}$ [FL^{-2}] equals (Fig. 3h):

$$t_{r,s} = \frac{(L_r - L_s)}{2}\frac{\tau_i C_r}{A_r} \tag{31}$$

Eq. (31) can be rewritten in terms of a quadratic polynomial that can be analytically solved for $t_{r,s}$:

$$\xi_2 t_{r,s}^2 + \xi_1 t_{r,s} + \xi_0 = 0 \tag{32}$$

Expressions for the coefficients, both for roots that behave fully elastically and elasto-plastic roots, are given in Table 2. Similar to 'anchored' roots, the tensile stress in 'slipping' roots $t_{r,s}$ can be found by first using the elastic solution, and if the calculated tensile stress exceeds the root yield stress, replacing this with the elasto-plastic solution.

Theoretically, it is possible that due to excessive slippage, the entire root ends up within the shear zone (i.e. when $L_r \cos\beta \leq h$). In this case, the tensile stress in the root is set to zero ($t_{r,s} = 0$).

The 'slipping' case is an upper-bound solution, always limiting the 'anchored' case. Therefore, the root tensile stress within the shear zone (in an intact root) t_r [FL^{-2}] can be found by taking the minimum tensile stress calculated by either of the mechanisms:

$$t_r = min\left(t_{r,a}, t_{r,s}\right) \tag{33}$$

d) Broken roots: In the previous calculations for the tensile stress in anchored and slipping roots, it is assumed that the roots do not break, i.e. $t_{r,u} = \infty$. Roots will however break if the tensile stress exceeds the root tensile strength $t_{r,u}$.

Breakage is incorporated in the model through applying a dimensionless reduction factor f_b:

$$f_b = \begin{cases} 1 & \text{when } t_r \leq t_{r,u} \\ 0 & \text{when } t_r > t_{r,u} \end{cases} \tag{34}$$

When a probabilistic model for root failure is used (similar to Eq. (4)):

$$f_b = exp\left(- \left[\Gamma\left(1 + \frac{1}{\kappa}\right)\frac{t_r}{t_{r,u}}\right]^{\kappa}\right) \tag{35}$$

necessitating a choice for Weibull shape parameter κ.

Once roots are broken, they cannot 'unbreak' if the root tensile stress reduces at a later stage. Therefore the analysis is run progressively by gradually increasing shear displacement u while monitoring the smallest value of the breakage parameter achieved so far for each root:

$$f_b = \min\left(f_{b,i}, f_{b,i-1}\right) \tag{36}$$

Table 2
Polynomial coefficients for calculating stresses in slipping roots (Eq. (32)).

Coefficient	Elastic solution	Elasto-plastic solution
ξ_2	$\frac{-1}{E_{r,e}}$	$\frac{-1}{E_{r,p}}$
ξ_1	$\frac{L_r}{2}\frac{\tau_i C_r}{A_r}\frac{1}{E_{r,e}} - 1$	$\frac{L_r}{2}\frac{\tau_i C_r}{A_r}\frac{1}{E_{r,p}} - 1 + \zeta$
ξ_0	$\frac{1}{2}\frac{\tau_i C_r}{A_r}\left[L_r - \frac{h}{cos\beta}\right]$	$\frac{1}{2}\frac{\tau_i C_r}{A_r}\left[L_r(1-\zeta) - \frac{h}{cos\beta}\right]$

where $f_{b,i}$ is the breakage parameter in the current step i, and $f_{b,i-1}$ the calculated breakage parameter in the previous shear displacement step.

Summary: All of the required equations to calculate the tensile stress in a root as a function of root properties, interface properties and shear displacements have now been defined. A flowchart of the methodology to calculate the root tensile stress is outlined in Fig. 4.

2.4. Thickness of the shear zone

Soil often shows highly localised shear deformations ('shear zone'). When roots are not present, the shear zone has an initial, finite thickness h_0 [L], which may be estimated using established soil mechanics theory, e.g. $h_0 \approx 10 d_{50}$, where d_{50} is the mean soil particle size (Oda and Iwashita, 1999). The available shear resistance of the non-rooted soil ($\tau_{s,u}$, [Pa]) can be calculated for example using the Mohr-Coulomb failure criterion:

$$\tau_{s,u} = c' + \sigma_n' tan\phi' \tag{37}$$

where c' is the apparent soil cohesion [FL^{-2}] and σ_n' the normal effective stress acting on the shear plane (without any additional root confinement, [FL^{-2}]). This may be substituted by suitable alternatives when dealing with partially saturated soils. The effect of changes in the hydrological state of the soil on slope stability, for example during rainfall infiltration, can be accounted for by changing the shear strength of the soil accordingly.

Experimental evidence suggests that mobilisation of root stresses causes the shear zone to increase in size, and not remain constant as assumed by Waldron (1977). The following approach was developed to capture this mechanism.

As roots start to mobilise strength, stress will be transferred from the root to the soil at the edge of the shear zone in a thin transition zone (Fig. 5) to accommodate the change in root orientation. Soil just outside the shear zone will be reinforced by the component of root tensile strength normal to the shear zone, but at the same time is destabilised by the component parallel to the shear direction. The net result is a destabilising shear stress that may cause the soil outside the current shear zone to yield. When roots are loaded in tension, $\beta > \beta_0$ and $\alpha > \alpha_0$. Therefore the largest destabilising shear stress the roots apply to the soil ($\tau_{s,r}$) in the transition zone equals (note similarities with WWM Eq. (15)):

$$\tau_{s,r} = \sum_i \phi_r t_r (cos\alpha sin\beta - cos\beta tan\phi') \tag{38}$$

When the destabilising load exceeds the shear strength of the soil ($\tau_{s,r} > \tau_{s,u}$), the soil on the edge of the current shear zone will yield, resulting in an increase in shear zone thickness h. The shear zone thickness will increase until $\tau_{s,r}$ has been sufficiently reduced so that $\tau_{s,r} \leq \tau_{s,u}$. This simple model thus allows for the shear zone thickness to increase as long as root stresses are sufficient to reach the yield stress in the soil outside the shear zone.

In the implementation of the model, a maximum shear band thickness h_{max} can be defined that cannot be exceeded. This can be useful for when modelling cases where the shear zone thickness is limited by boundary conditions, for example in direct shear conditions, or when modelling roots reinforcing across a fabric feature such as a discontinuity filled with a weak infill material. In addition, it should be noted that the case $h = h_0 = h_{max} = 0$ is equivalent with modelling the opening of a tensile crack, for example at the top of a landslide scarp.

2.5. Summary and numerical implementation

The root reinforcement as a function of soil shear displacement u_s can be established by coupling the newly developed model components together.

At the current amount of soil shear displacement u_s, calculate the (deformed) root orientations (α, β), root tensile stresses (t_r) and breakage

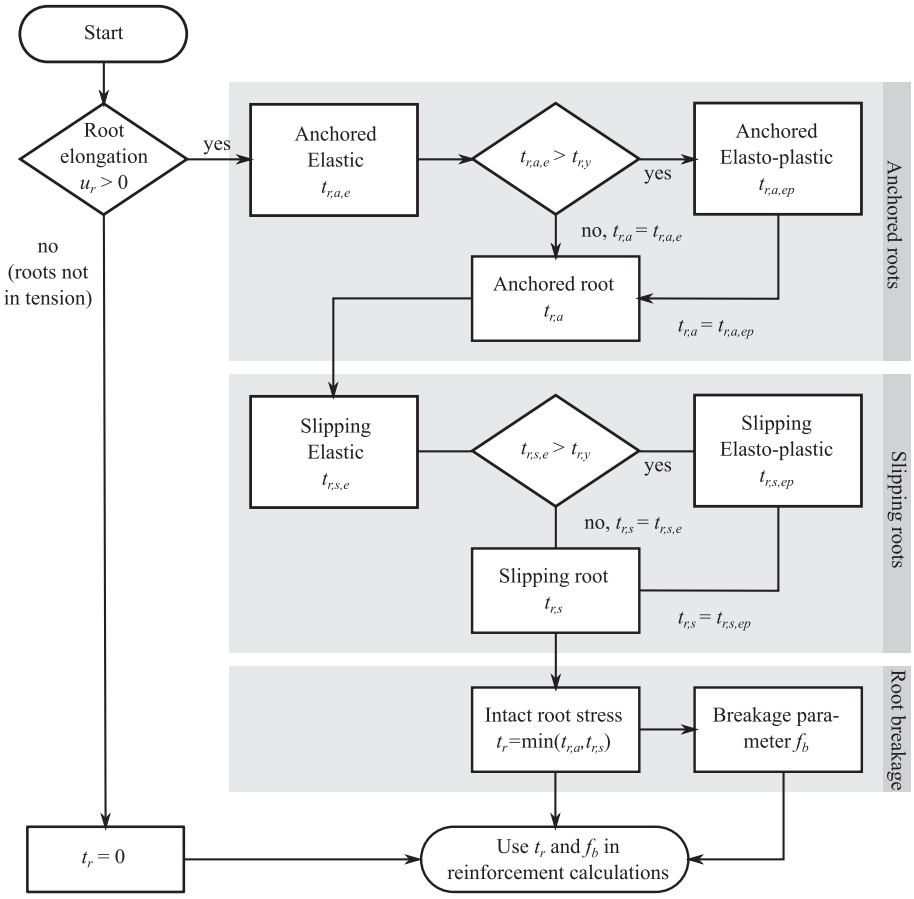

Fig. 4. Flowchart for calculation of the current root tensile stress t_r given the current stresses and displacements in the soil.

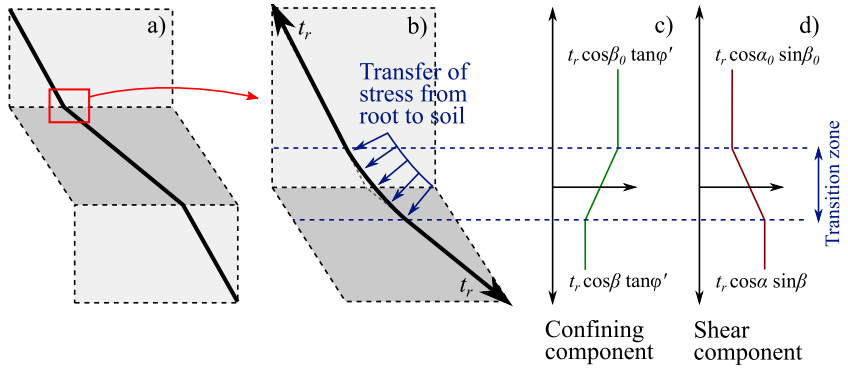

Fig. 5. Transition of stress from root to soil at the edge of the shear zone, potentially destabilising the previously not yielding soil just outside the shear zone.

parameters (f_b) for each root. Subsequently calculate the current reinforcement c_r by summing the contributions of all roots i:

$$c_r = \sum_i \phi_r t_r f_b (cos\alpha sin\beta + cos\beta tan\phi') \quad (39)$$

The full root reinforcement versus shear displacement behaviour is found by progressively increasing u_s while updating shear zone thickness h as required, see Fig. 6. The peak root reinforcement $c_{r,u}$ can subsequently be obtained by finding the maximum reinforcement c_r within the range of shear displacements.

This approach is computationally very efficient, as all equations are expressed analytically. The only numerical procedure required is finding the new value of shear zone thickness h in case the soil outside the shear zone is unstable, which can be done by solving $\tau_{s,u} = \tau_{s,r}$.

The model was implemented in the free software R (R Core Team, 2013), and can be found online (Meijer, 2022) [insert reference to GitHub repository after paper acceptance]. An online app showcasing the model can be found on https://gjmeijer.shinyapps.io/DRAM/

3. Methods: comparison with experimental data

The predictions by the DRAM were validated against two independent sets of direct shear tests.

3.1. Direct shear tests by Liang et al. (2017)

Liang et al. (2017) conducted a series of direct shear experiments on soil reinforced with *Salix viminalis* (willow, variety Tora), *Lolium perenne*

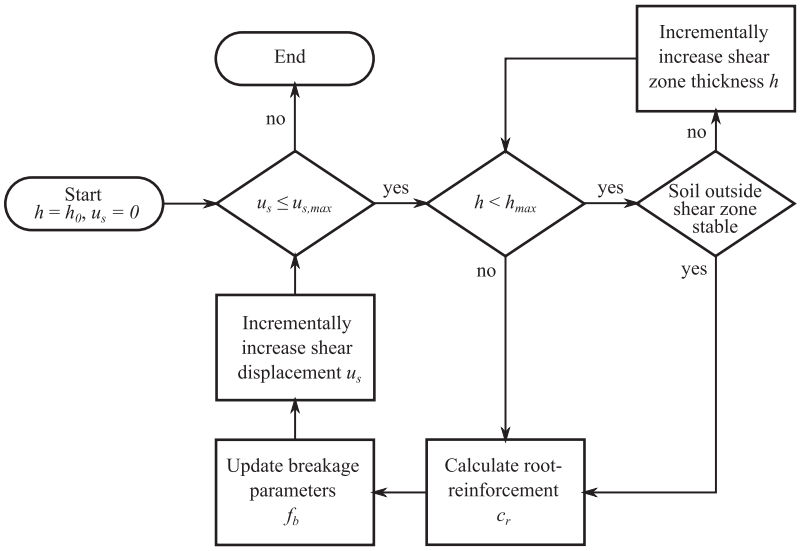

Fig. 6. Flowchart for calculation of root reinforcement c_r as function of a increasing direct shear displacements u_s in the soil.

× *Festuca pratensis* (festulolium grass) or *Ulex europaeus* L. (gorse) roots. 150 mm diameter cores with a height of 500 mm were filled with recompacted Bullionfield field soil (mineral portions consisting of 71% sand, 19% silt and 10% clay; dry density $\rho_d = 1.4$ Mg m^{-3}), planted and grown for 2–3 months, fully saturated and then drained to 5 kPa matric suction at surface level, and subsequently sheared at 100, 200, 300 or 400 mm depth. For more details on test preparation and setup, see Liang et al. (2017), and for detailed data on root counts and shear displacement–shear stress traces for both rooted and fallow samples, see Meijer et al. (2021). The average fallow soil shear strength was measured as $\tau_{s,u} = 2.7$ kPa with no depth trend, with a soil angle of internal friction $\phi' = 36.4°$.

As roots were grown in relatively slender cores, in DRAM predictions all roots were assumed to have grown vertically from the top to the bottom of the core ($L_r = 500$ mm, $\alpha_0 = \beta_0 = 0°$). The soil–root interface was assumed to be rough such that $\tau_i = \tau_{s,u}$. Root yield stresses and strains were determined by fitting the experimentally measured stress-strain curves bilinearly (Fig. 7).

All root biomechanical parameters are presented in Table 3, using power-law relationships for both root tensile strength and tensile strain to failure:

$$t_{r,u} = t_{r,u,0}\left(\frac{d_r}{d_{r,0}}\right)^{\beta_t} \tag{40}$$

$$\varepsilon_{r,u} = \varepsilon_{r,u,0}\left(\frac{d_r}{d_{r,0}}\right)^{\beta_\varepsilon} \tag{41}$$

where $d_{r,0}$ is a reference diameter [L], and $t_{r,u,0}$ [FL^{-2}] and $\varepsilon_{r,u,0}$ [LL^{-1}] the tensile strength and tensile strain to peak for roots with this diameter respectively. The measured variation in root tensile strength was captured by fitting a Weibull distribution to the normalised tensile strength (ratio of measured versus power-law prediction), resulting in shape parameters κ_t (see Meijer, 2021). It was assumed that the probabilistic distribution of root failure is fully driven by the variation in root tensile strength, so $\kappa = \kappa_t$ in Eq. (35).

The initial shear zone thickness was chosen as $h = 2$ mm ($h_0 \approx 10 d_{50}$) or $h = 30$ mm (in line with the maximum thickness observed in X-ray CT observations by Bull et al. (2020)). Predictions for the shear displacement–shear stress behaviour of the rooted soil were acquired by adding the predicted reinforcement to the average fallow soil behaviour measured at each shear plane depth.

3.2. Direct shear tests by Bull et al. (2020)

Bull et al. (2020) performed a similar series of direct shear experiments using the same soil and plant species. Five tests were conducted on both willow (replicates C, E, F, H and I) and gorse-planted cores (replicates A, B, G, J and K). Smaller (103 mm diameter, 500 mm high) cores were sheared at 250 mm depth under approximately 5 kPa of suction (at the soil surface). After each test, the diameters of all roots crossing the shear plane were recorded (Fig. 8). Cores were sheared to a maximum displacement of 20 mm. Some tests were conducted in the μ-VIS X-Ray micro-CT scanner at the University of Southampton, stopping seven times at points regularly spaced along the displacement

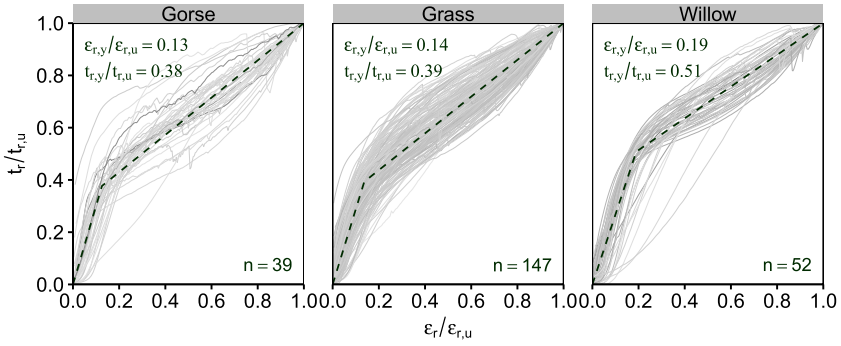

Fig. 7. Elasto-plastic bilinear approximation of root tensile strain versus tensile stress response. Each grey solid line (total number of lines: n) indicates a single tensile test conducted by Liang et al. (2017).

Table 3
Root biomechanical properties measured by Liang et al. (2017) and analysed by Meijer. (2021). The reference diameter $d_{r,0} = 1$ mm was used during fitting.

Species	Tensile strength			Tensile strain to failure		Yield strength	Yield strain
	$t_{r,u,0}$ [MPa]	β_t [−]	κ_t [−]	$\varepsilon_{r,u,0}$ [mm/mm]	β_ε [−]	$t_{r,y}/t_{r,u}$ [−]	$\varepsilon_{r,y}/\varepsilon_{r,u}$ [−]
Gorse	22.8	0.0697	2.13	0.178	0.0769	0.38	0.13
Grass	6.25	−0.655	2.46	0.320	0.100	0.39	0.14
Willow	10.8	0.0291	1.81	0.239	−0.0934	0.51	0.19

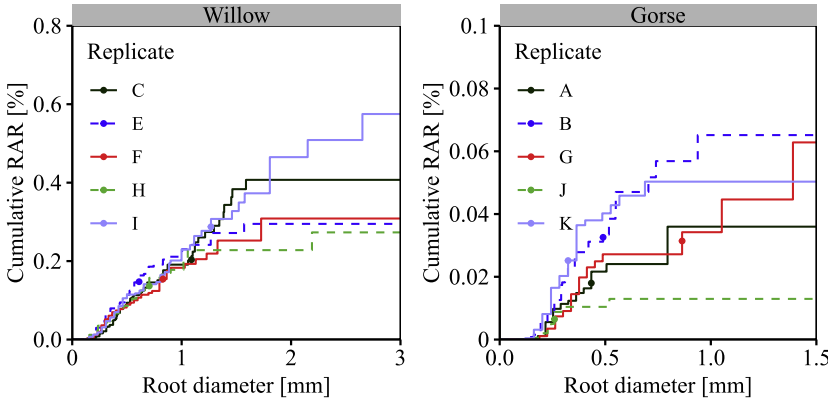

Fig. 8. Cumulative root area ratio (*RAR*) measured on shear planes after direct shear testing by Bull et al. (2020). Dots indicate the root diameter at 50% of the maximum *RAR*.

interval to perform a scan. These stops caused some (temporary) relaxation in shear stress which was regained when shearing recommenced. Digital volume correlation was applied to the X-ray CT dataset to obtain full field displacement and strain information in 3D. This allowed a direct method of measuring the shear zone thickness (Bull et al., 2021).

The same set of soil and root parameters was used as in modelling of tests by Liang et al. (2017). Measured fallow soil shear strengths were slightly larger ($\tau_{s,u} = 3.3$ kPa) and therefore $\tau_i = 3.3$ kPa was assumed.

3.3. Comparison to existing displacement-driven models

The experimentally measured shear displacement versus root reinforcement traces were furthermore compared to the RBMw (Schwarz et al., 2013) and the models by Waldron (1977) and Waldron and Dakessian (1981) described in the introduction section, using the same root and soil parameters as in the DRAM. In these models the (linear elastic) root stiffness was set to the Young's modulus $E_{r,e}$. In the RBMw, $\kappa = \kappa_t$ was assumed, as well as $k' = 1.2$ and $u_s = u_r$ to account for direct shear rather than pullout conditions. For each model, the total predicted shear resistance of the rooted soil was determined by adding the calculated reinforcement to the average experimentally measured shear stress in the non-rooted ('fallow') soil.

The difference between measured and predicted reinforcements was quantified for each direct shear tests using two parameters:

- $|\Delta c_r|_{,max}$: The maximum absolute difference between measured and predicted reinforcement, anywhere along the entire shear displacement range.
- $|\Delta c_r|_{,avg}$: The average absolute difference between measured and predicted reinforcement, averaged across the entire shear displacement range.

Both parameters should be close to zero for a model to accurately predict both reinforcement mobilisation and peak reinforcement. The temporarily reduced shear stresses associated with a pause in shearing to enable X-ray CT scanning during some tests by Bull et al. (2020) were ignored during calculation of these summary parameters.

4. Results

Both sets of experiments show a large increase in the shear resistance in rooted soil. Direct shear experiments by Bull et al. (2020) could be well matched with the model (Fig. 9) when an initial shear zone thickness of $h_0 = 2$ mm was assumed. Both the initial stiffness as well as the observed decrease in stiffness after $u_s > 2$–3 mm was well captured. Increasing the initial shear zone thickness h_0 to 30 mm resulted in a much more gradual mobilisation of root stress and less accurate reinforcement predictions (Table 4). In the case of $h_0 = 2$ mm, for most tests the shear zone thickness was predicted to increase during shearing, indicating enough root material was present to affect the behaviour of the soil (Fig. 10). In Willow test F, in contrast to all other tests, the plant shoot was not removed prior to shearing, resulting in drier and therefore stronger soil. This explains why root reinforcements were underestimated for this test.

The predicted reinforced shear displacement–shear stress traces also matched the experiments by Liang et al. (2017) well (Fig. 11). Although the peak reinforced shear stress was hardly affected by the choice of initial shear zone thickness (±0.25 kPa), the mobilisation of this reinforcement was. In most tests, assuming $h_0 = 30$ mm provided better predictions compared to $h_0 = 2$ mm (Table 4), although in some individual tests this behaviour was reversed. Tests conducted closer to the soil surface, containing more root material, showed that shear zone thickness might increase significantly during the test (Fig. 12).

In some experiments (notably the gorse replicate J test by Bull et al. (2020), and gorse sheared at 400 mm depth tested by Liang et al. (2017)) no reinforcement was measured despite the presence of significant amounts of root material. This inevitably led to overestimation of root reinforcement. In several of the tests on gorse, roots may have extended only slightly below the shear zone, leading to insignificant root reinforcements due to root slippage. For grass replicate 2 sheared at 200 mm depth by Liang et al. (2017), the measured reinforcement

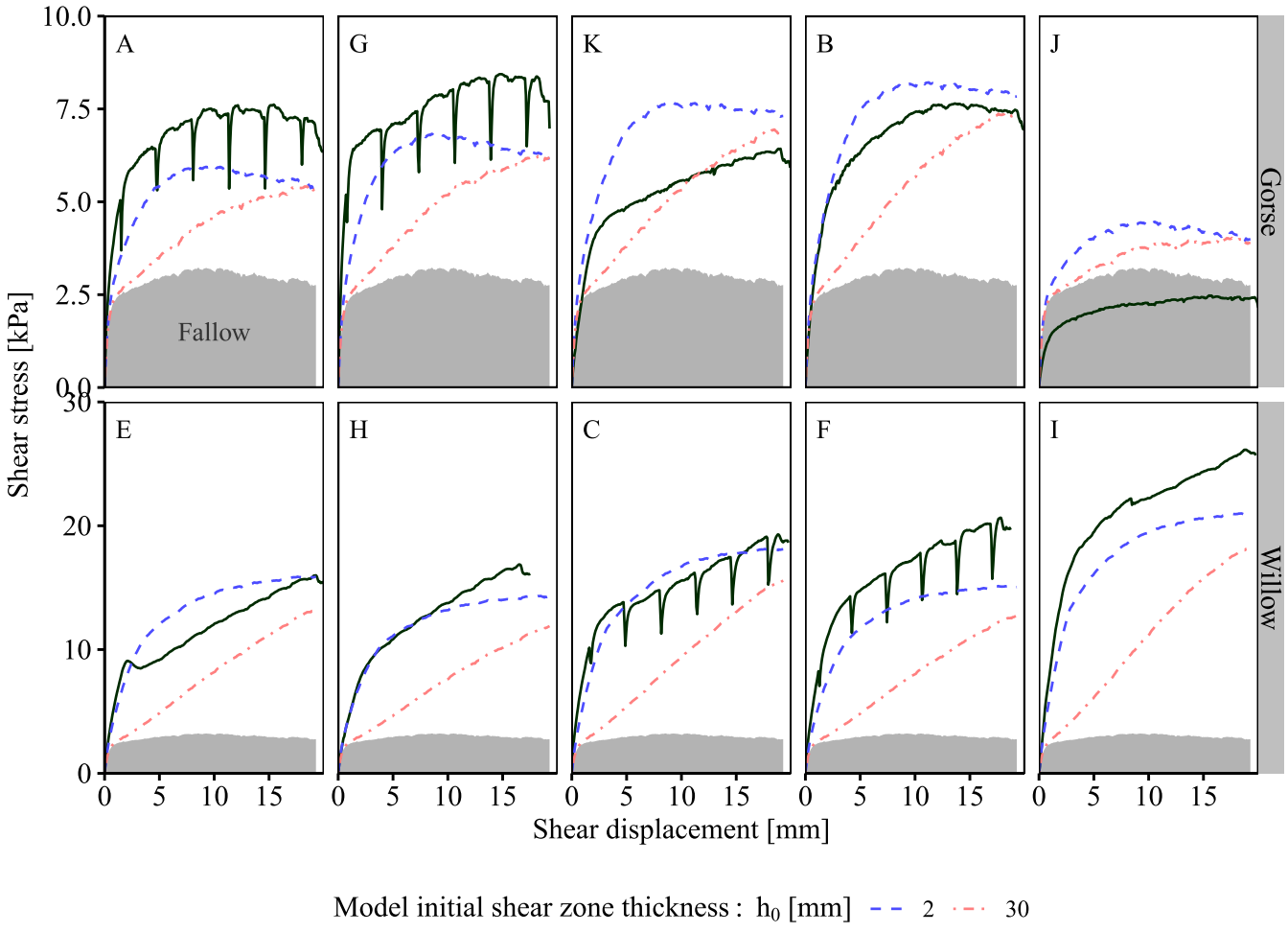

Fig. 9. Measured and predicted direct shear displacement–shear stress traces for tests performed by Bull et al. (2020). Predictions are made using different assumptions of the initial shear zone thickness h_0. Solid lines indicate the experimentally measured root-reinforced response, while the shaded grey area indicates the average experimental shear stress measured in fallow soil.

Table 4
Mean and standard deviations of the maximum ($|\Delta c_r|_{,max}$) and average ($|\Delta c_r|_{,avg}$) absolute difference between experimental and DRAM predictions of root reinforcement for each test.

Study	h_0 [mm]	$\|\Delta c_r\|_{,max}$ [kPa]	$\|\Delta c_r\|_{,avg}$ [kPa]
Bull et al. (2020)	2	2.96 ± 1.39	1.76 ± 1.00
	30	5.74 ± 4.03	4.25 ± 3.24
Liang et al. (2017)	2	3.22 ± 1.72	1.43 ± 1.03
	30	2.17 ± 1.68	1.28 ± 1.05

appears almost zero. It was hypothesised that the soil component of the direct shear resistance must have been lower than expected since roots must have been present at this depth given the measured root reinforcement at larger depths (300 and 400 mm) in the same core.

The experimental results show that significant reinforcement is still present at large shear displacements, suggesting many roots might slip rather than break. This is confirmed by DRAM predictions, showing only a relatively small fraction of roots (10–25% on average) had failed at the end of shearing (Fig. 13). All roots initially behaved as 'anchored' roots, but increasing shear displacements caused them to either break or slip. Fig. 13 further shows predictions that a significant fraction of roots were strained beyond the yield strain, resulting in plastic root behaviour in the shear zone.

Similar to the DRAM, the root reinforcement models by Waldron (1977) and Waldron and Dakessian (1981) matched the initial reinforced soil stiffness well (Fig. 14). At larger displacement however both predicted larger reinforcements since they do not include stiffness-reducing effects such as root plasticity or the gradual increase in shear zone thickness. The inclusion of slippage in Waldron and Dakessian (1981) reduced the predicted reinforcement beyond a certain shear displacement ($u_s \gtrsim$ 7–13 mm in Fig. 14) compared to the model by Waldron (1977). The RBMw typically struggled to accurately predict the stiffness of the rooted soil measured in the experiments, and furthermore predicted a gradual reduction of reinforcement after reaching the peak reinforcement caused by the underlying model assumption that all roots will eventually break.

The difference between measured and predicted reinforcement using the various models was investigated in more detail by analysing $|\Delta c_r|_{,max}$ and $|\Delta c_r|_{,avg}$. Average values across all tests (Fig. 15) shows that the DRAM performed best on both criteria ($|\Delta c_r|_{,max} \approx$ 2.7–3.0 kPa, $|\Delta c_r|_{,avg} \approx$ 1.3–1.8 kPa), followed by the model by Waldron and Dakessian (1981) (3.3–4.0 kPa, 1.8–1.9 kPa), the RBMw (4.5–4.7 kPa, 2.3–2.5 kPa) and finally the model by Waldron (1977) (4.9–5.1 kPa, 2.2–2.9 kPa).

Peak reinforcements $c_{r,u}$ were further compared against those obtained with ultimate limit state models such as the WWM and various FBMs (Fig. 16). On average, DRAM predictions were 3 to 16% lower compared to measured root reinforcements. The WWM overestimated measured reinforcements by around 180%, while the RBMw and the

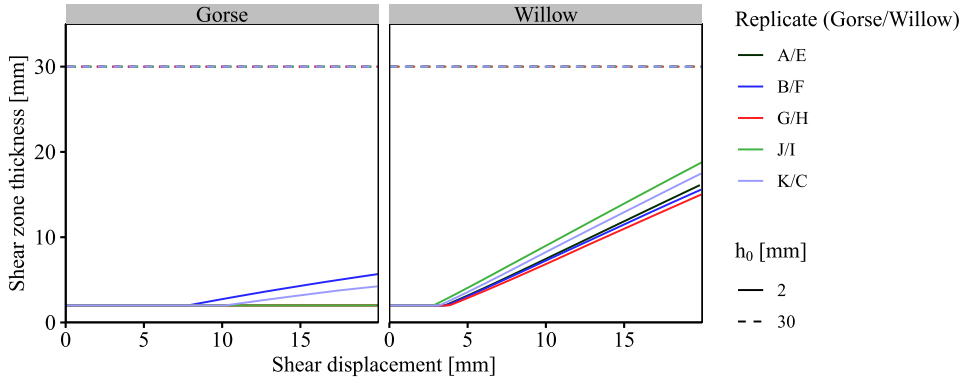

Fig. 10. Evolution of shear zone thickness h in model predictions for direct shear tests performed by Bull et al. (2020), using different values for the assumed initial shear zone thickness h_0. All curves for the case $h_0 = 30$ mm overlap (dashed lines), and so do curves for Gorse replicates I and K in the case of $h_0 = 2$ mm (solid lines).

models by Waldron (1977) and Waldron and Dakessian (1981) overestimated by lesser amounts (18–37%, 46–104% and 4–46% respectively). FBM predictions showed a wide range (8% underestimation to 166% overestimation) depending on the chosen load sharing mechanism (β_F).

5. Discussion

The newly developed model (DRAM) yielded good predictions for both the mobilisation and the magnitude of root reinforcement for the experiments considered. These experiments showed a limited reduction in reinforcement after reaching the peak reinforcement, similar to behaviour observed in direct shear tests (e.g. Ekanayake et al., 1997; Fan and Su, 2008). This behaviour indicates that many roots may have slipped rather than broken, which was confirmed by the DRAM (Fig. 13) and in line with recent experimental observations (Zhu et al., 2020). Compared to field conditions, the number of slipping roots may be exacerbated by laboratory testing methods. The latter used relatively small samples with younger, relatively short roots in combination with lower confining stresses, which may result in less root confinement and therefore more slippage compared to the field.

The importance of slipping roots in the experiments explains why displacement-driven models that do not include root slippage (RBMw and the model by Waldron (1977)) performed worse than those that did (DRAM and the model by Waldron and Dakessian (1981)). The differences between the DRAM and the model by Waldron and Dakessian (1981) furthermore shows that the inclusion of root plasticity and a dynamically increasing shear zone thickness — aspects not previously considered — may further reduce the predicted reinforcement to levels closer to experimental observations.

While the DRAM and models by Waldron (1977) and Waldron and Dakessian (1981) yielded good predictions for the initial stiffness of the rooted soil, the RBMw by Schwarz et al. (2013) was less accurate. It is hypothesised that this was caused by the assumed mobilisation mechanism of root strength. The RBMw assumes all roots stretch evenly along the entire root length, rather than the root stress being initially concentrated near the shear zone only, and does not take into account the interaction with the surrounding soil (e.g. root–soil interface resistance τ_i). Furthermore, the additional assumptions required to transition from pullout to direct shear conditions ($k' = 1.2$, $u_r \approx u_s$) will have effected the (initial) stiffness.

The experiments show that peak root reinforcements occurred at large shear deformations (of the order of 50 mm). This has significant implications for the way peak root reinforcement is defined. In previous studies, peak root reinforcement is almost always defined as the difference between the peak shear strengths of rooted and fallow soils (e.g. Fan and Su, 2008), subsequently called 'apparent reinforcement'. In contrast, traditional root reinforcement models such as the WWM or FBM calculate the 'actual reinforcement', the largest difference between rooted and unrooted strength occurring at any displacement level, see Fig. 17. Since shear displacements to reach peak strengths in rooted soils are much larger than in fallow soils (Ekanayake et al., 1997; Fan and Su, 2008; Mickovski et al., 2009), at these larger displacements the soil strength may have reduced towards a critical state or residual strength (common in field soils due to soil ageing or cementation (Utomo and Dexter, 1981) and observed in the field by Meijer et al. (2018)). Thus, adding calculated peak root reinforcements (for example calculated using the WWM, FBM) to peak soil strength may lead to substantial overestimation of the shear strength of root-reinforced soil which is unconservative in stability analyses at the ultimate limit state. A better and more conservative practice would be to add $c_{r,u}$ to the residual soil strength instead. Models that can calculate root reinforcement as a function of shear displacement, such as the newly developed DRAM, are able to address this inconsistency as they can provide predictions for the 'actual reinforcement' instead that can be added to soil stress-deformation curves. Since such models can be validated against full displacement versus reinforcement traces, rather than the 'apparent' peak reinforcements only, there can be greater confidence that they will yield reliable predictions and better capture the complicated interaction between soil and root.

The direct shear experiments used to validate the DRAM had a number of limitations. Test were performed on relatively young and thin roots ($d_r \leq 3.2$ mm). The DRAM, similar to many of the other models discussed, assumes roots can only sustain tensile forces, making it potentially less suitable for thicker roots with significant resistances to bending. To model the effect of bending and/or branching in thicker roots, such as may be present in large tree root architectures, different and more sophisticated models are required (e.g. Wu et al., 1988; Meijer et al., 2019a; Meijer et al., 2019b).

The experiments used to validate the DRAM used plants grown in relatively slender cores, causing roots to cross the shear zone more or less perpendicularly. The root orientation part of the DRAM could therefore not be validated. While this part of the model is a logical geometrical extension, further validation is required using samples with more widely varying root orientations. Previous work has shown that roots orientations may have a significant effect of the mobilisation and magnitude of reinforcement (Gray and Ohashi, 1983; Jewell and Wroth, 1987; Fan and Chen, 2010; Thomas and Pollen-Bankhead, 2010).

The potential increase in shear zone thickness with increasing deformations was difficult to validate. While this is likely to occur during landsliding conditions, it is difficult to study this mechanism using a shear box because of the discontinuous displacement boundary conditions applied. Indeed, previous studies of fibre-reinforced soils found that the size of the shear box may affect the shear zone thickness

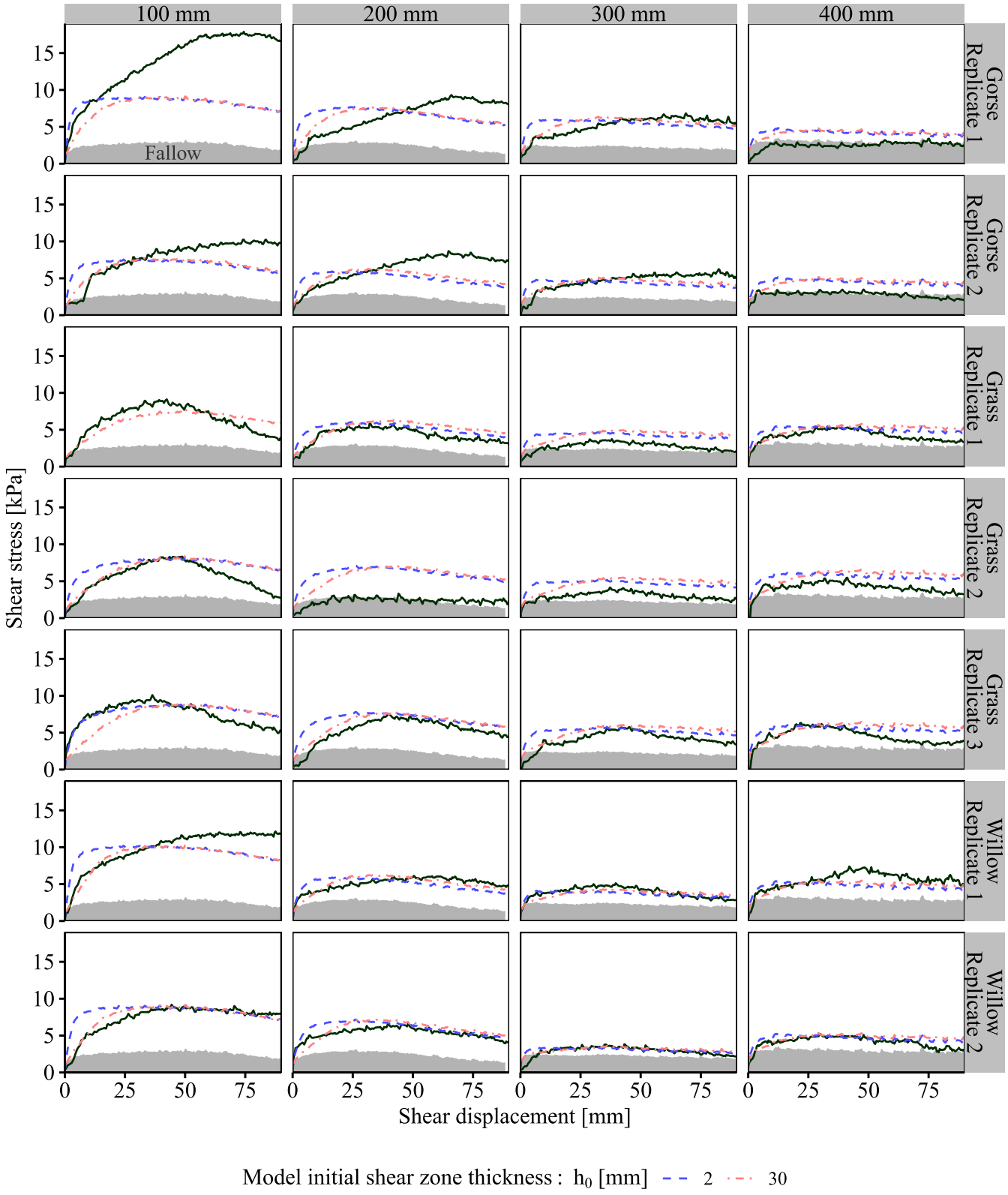

Fig. 11. Measured (dark green, solid line) and predicted (dashed and dash-dotted lines) direct shear displacement–shear stress traces for tests performed by Liang et al. (2017). Predictions are made using different assumptions of the initial shear zone thickness h_0. Grey shaded areas indicate the average fallow behaviour at each shear plane depth. (For interpretation of the references to color in this figure legend, the reader is referred to the web version of this article.)

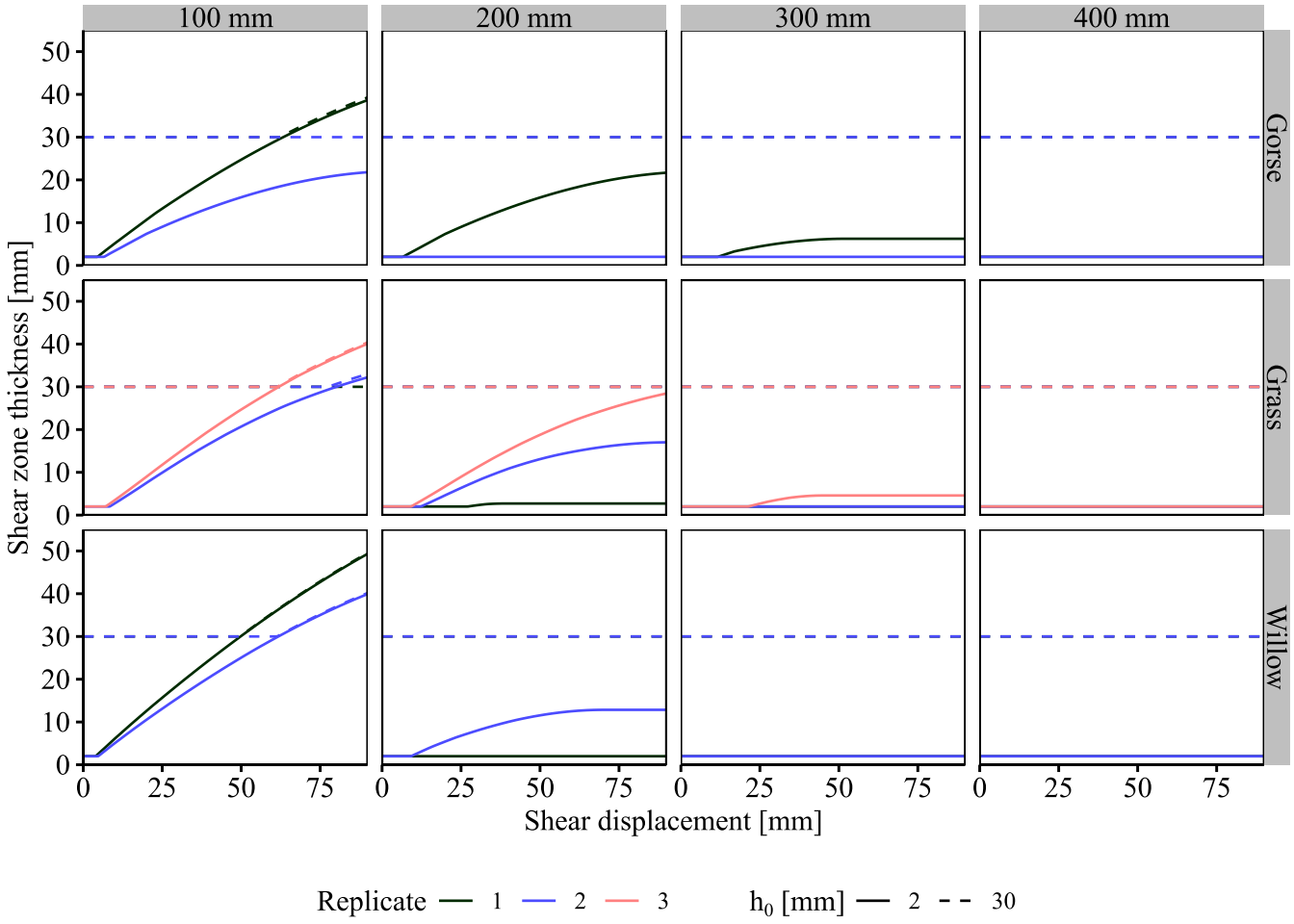

Fig. 12. Predicted shear zone thickness as function of shear displacement for tests performed by Liang et al. (2017), using different values for the assumed initial shear zone thickness h_0. Note that many curves for the case $h_0 = 30$ (dashed lines) mm overlap, as do some curves for $h_0 = 2$ mm (solid lines).

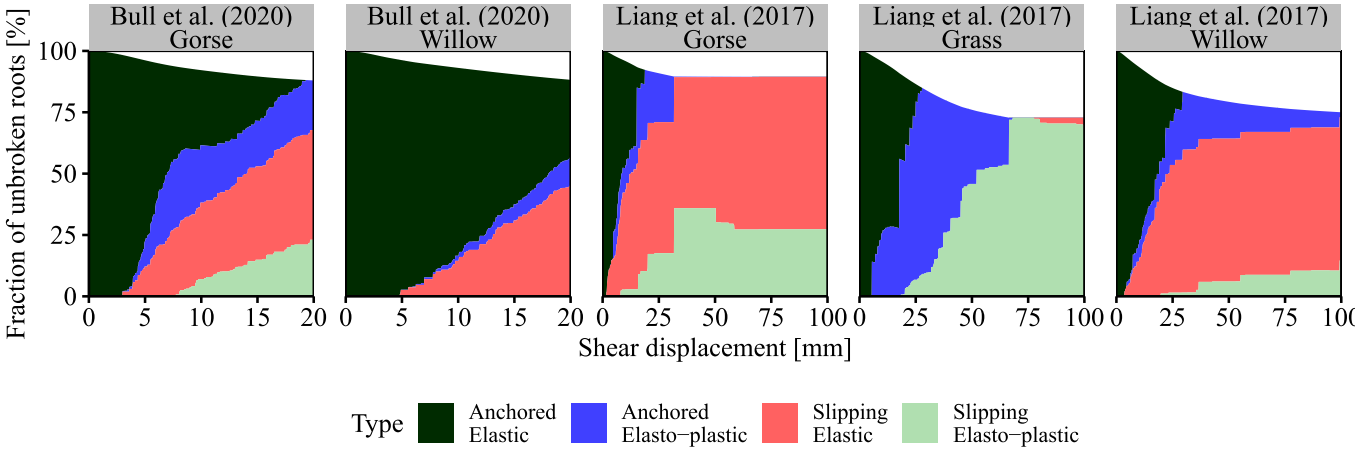

Fig. 13. Predicted average percentages of the initial root area ratio that remains intact as function of shear displacement. The percentage of intact roots is further subdivided between different types of root behaviour. $h_0 = 2$ and $h_0 = 30$ mm was assumed for tests by Bull et al. (2020) and Liang et al. (2017), respectively.

(Shewbridge and Sitar, 1989). Both the model simulations described here, showing the effect of shear zone thickness on the mobilisation of root reinforcement, as well as previous experimental observations of shear zone thickness in rooted direct shear tests demonstrate the importance of understanding this interaction, which so far has been overlooked in the literature. While this part of the model can easily be switched off by specifying a constant shear zone thickness ($h = h_0 = h_{max}$), similar to Waldron (1977) and Waldron and Dakessian

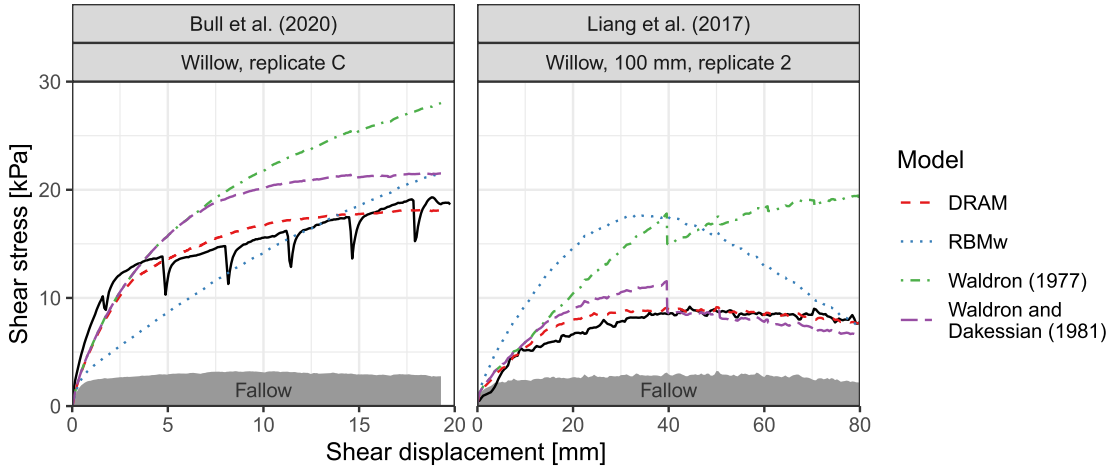

Fig. 14. Example experimental and model shear displacement versus root reinforcement traces. Solid lines indicate the experimentally measured shear stress in the rooted soil. $h_0 = 2$ and $h_0 = 30$ mm was assumed for tests by Bull et al. (2020) and Liang et al. (2017) respectively.

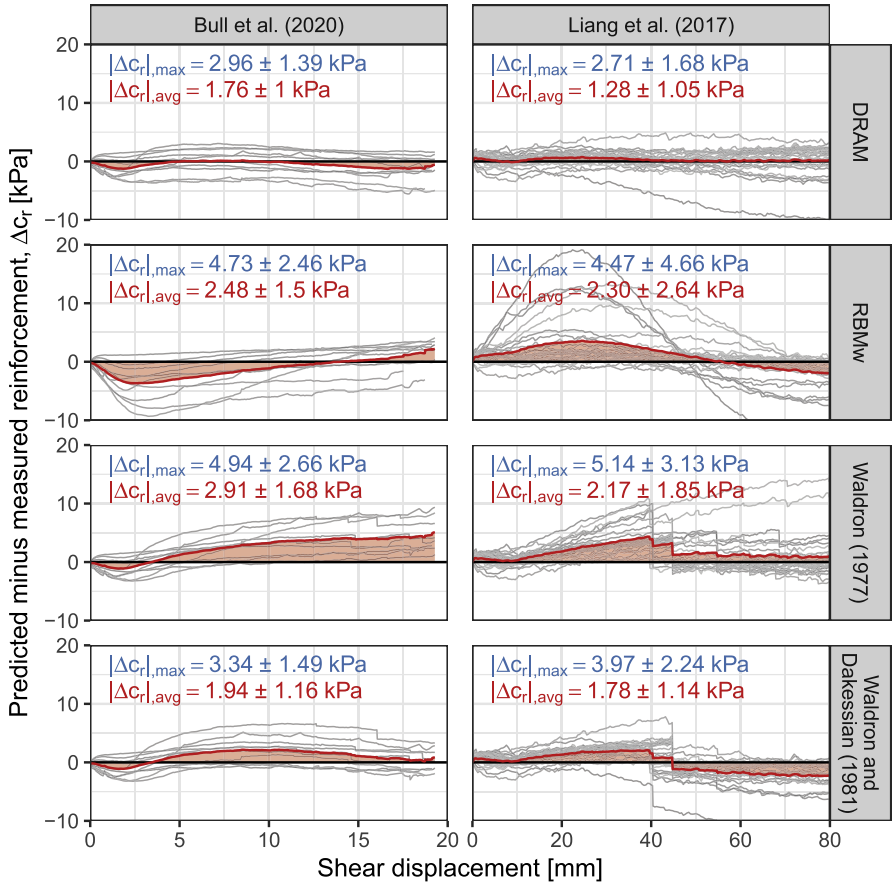

Fig. 15. Differences between predicted (models) and measured (experiments) root reinforcement, as a function of direct shear displacement u_s. Means and standard deviations for $|\Delta c_r|_{,max}$ and $|\Delta c_r|_{,avg}$ are shown using annotations. Thin grey lines indicate individual test results. Thick red lines indicate the average difference across all tests. $h_0 = 2$ and $h_0 = 30$ mm was assumed for tests by Bull et al. (2020) and Liang et al. (2017) respectively. (For interpretation of the references to color in this figure legend, the reader is referred to the web version of this article.)

(1981), future work should investigate this interaction between the presence of roots and the soil failure mechanism more closely.

Bull et al. (2020) observed a preferential growth of root material near the sides of the core, where the shear zone thickness was much smaller ($h \approx 2$ mm) than in the centre of the core ($h \approx 30$mm). This explains why the model assuming an initial shear zone thickness of $h_0 = 2$ mm performed best. In contrast, Liang et al. (2017) used both larger cores and cut all roots growing adjacent to the core side with a scalpel blade before commencing shear testing, which may explain why in most tests assuming a thicker initial shear zone produced better predictions.

The DRAM only requires input parameters that are physically meaningful and measurable. Root biomechanical properties can be measured using uniaxial tensile testing (e.g. Loades et al., 2013), root volume fractions and diameters can be measured from obtaining soil cores (Genet et al., 2008) or trench wall methods (Moos et al., 2016), while root lengths may be measured on excavated roots or estimated based on root diameters (e.g. Giadrossich et al., 2013). The most

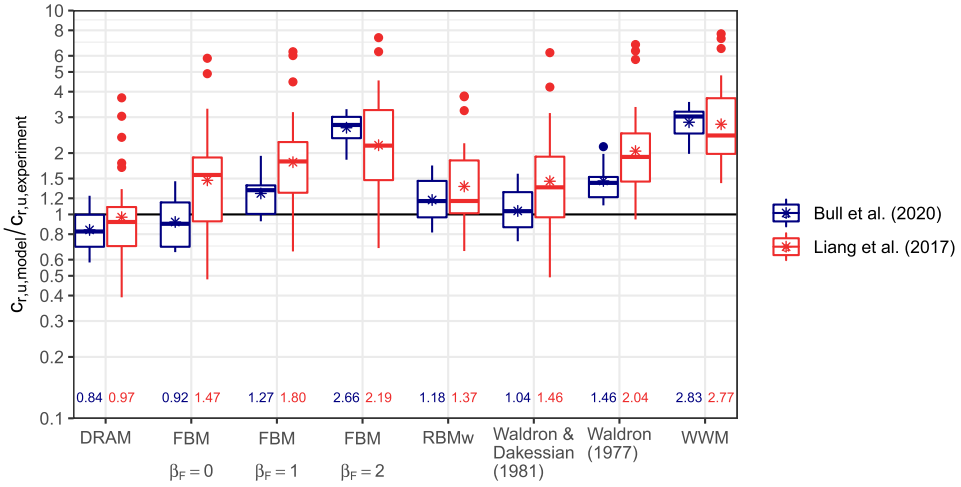

Fig. 16. Boxplots of the ratios between experimental and model predictions of peak root reinforcements $c_{r,u}$ (logarithmic scale) for different root reinforcement models. For each model and data source, the mean (geometric) values of the ratio are shown in the bottom of the figure and indicated by a star (*) in each boxplot.

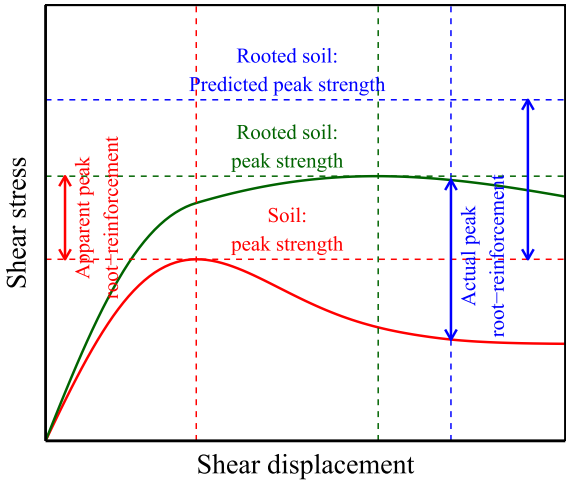

Fig. 17. Different definitions of root-reinforced shear strength. The 'apparent root-reinforcement' is the difference between the maximum shear stress in the rooted soil (green curve) and the maximum shear stress in the fallow soil (red curve). If the 'actual peak root reinforcement' (the largest difference between the two curves, i.e $c_{r,u}$) at large displacement is added to the peak fallow soil shear strength at small displacement, then the predicted maximum strength of the rooted soil may be substantially overestimated in soils that show softening behaviour. (For interpretation of the references to color in this figure legend, the reader is referred to the web version of this article.)

challenging input parameters to determine are (a) the spatial orientations of roots (α_0, β_0), which may be measured experimentally, for example using pinboards (Smit et al., 2000), or estimated using root architecture models (e.g. 'OpenSimRoot', Postma et al., 2017), and (b) the root–soil interface friction (τ_i), which may be estimated using pull-out testing (Schwarz et al., 2011) or geotechnical piling methods (e.g. Meijer et al., 2019a). The newly developed model can be used to study the effect of each of these root, soil and root–soil interface parameters on the magnitude and progressive mobilisation of root reinforcement independently, and thus provides a useful framework for future research.

The DRAM uses many of the same parameters used in existing displacement-driven models such as Waldron and Dakessian (1981) or the RBMw, see Table 5. In fact, when all roots are assumed linear elastic and initially perpendicular to the shear plane ($\beta_0 = 0°$), Weibull probability of root failure is not taken into account (i.e. $\kappa = \infty$) and the shear zone thickness remains constant (i.e. $h = h_0 = h_{max}$), the DRAM almost fully collapses to the original model by Waldron and Dakessian (1981). The only new parameters in the DRAM are the initial root orientations and, in case root elasto-plasticity is considered, a more accurate description of the root tensile elasto-plastic behaviour which could be obtained from the tensile tests conducted to measure root strength. This compatibility with existing approaches makes it a suitable and practical alternative to existing methods for use in slope stability assessment methods.

6. Conclusions

- A new analytical model ('DRAM') for calculating mechanical root reinforcement as a function of soil direct shear displacement was developed;
- The model incorporates the effects of root geometry (3-D root orientations, root diameters, root lengths), root biomechanics (elasto-plastic tensile stress–strain behaviour), failure dynamics (root breakage and/or slippage) and the effect of the surrounding soil (soil–root interface friction, shear zone thickness). The model closely follows the underlying physics of root strength mobilisation;
- The model showed good comparison with shear stress–displacement data measured in direct shear tests on for rooted soils. It matched both the magnitude and gradual mobilisation of root reinforcement, as well as the significant 'residual' root reinforcement at large deformations associated with slipping roots;
- The DRAM provided better predictions of experimentally measured direct shear displacement versus root reinforcement traces compared to existing displacement-driven reinforcement models. While the model by Waldron and Dakessian (1981) provided reasonable predictions, models that did not include root slippage such at the Root Bundle Model (RBMw) or the original model by Waldron (1977) yielded less accurate predictions.
- This newly developed model will be a useful tool for providing further insight into the key parameters controlling the gradual mobilisation of root reinforcement. Its ability to both provide accurate predictions for root reinforcement and the associated displacements required to mobilise reinforcements make it useful for both ultimate limit state and serviceability limit state problems.

Funding statement

This research was funded by EPSRC grant EP/M020355/1, which is a

Table 5
Input parameters required to calculate the root-reinforced soil strength under direct shear loading conditions, using different reinforcement models.

Group	Parameter	Displacement-driven models				Peak reinforcement models	
		DRAM	Waldron (1977)	Waldron and Dakessian (1981)	RBMw	WWM	FBM
Root geometry	Root diameters (d_r)	✓	✓	✓	✓	✓	✓
	Root quantities/root area ratio (ϕ_r)	✓	✓	✓	✓	✓	✓
	Root lengths (L_r)	✓		✓	✓		
	Initial root orientations (α_0, β_0)	✓					
Root biomechanics	Root tensile stiffness (E_r)	✓[a]	✓[b]	✓[b]	✓[b]		
	Root tensile strength ($t_{r,u}$)	✓	✓	✓	✓[c]	✓	✓
	Root breakage probability – Weibull (κ)	✓			✓		
Soil properties	Soil shear strength ($\tau_{s,u}$, or c', ϕ' and σ_n')	✓	✓	✓	✓	✓	✓
	Shear zone thickness (h or h_0)	✓	✓	✓			
	Root–soil interface resistance (τ_i)	✓	✓	✓			
	Shear displacement–root elongation relation ($u_s \sim u_r$)				✓[d]		
Other parameters	WWM multiplication factor (k')	[e]	[e]	[e]	✓[d]	✓	✓
	Load sharing parameter (β_F)						✓

[a] Linear elastic or linear elasto-plastic root behaviour.
[b] Linear elastic root behaviour only.
[c] Related to chosen Weibull scale parameter λ^*.
[d] Not commonly used, but may be required to covert the RBMw to direct shear conditions.
[e] k' is not a required input parameter, but is calculated instead using the direct shear displacement u_s, shear zone thickness h, soil friction angle ϕ' and the initial root orientations.

collaboration between the University of Dundee, the University of Southampton, the University of Aberdeen, Durham University and The James Hutton Institute. μVIS X-ray imaging work was supported by EPSRC grant EP/H01506X. The James Hutton Institute receives funding from the Scottish Government (Rural & Environmental Services & Analytical Services Division).

Data availability statement

R source code, including an interactive app showcasing the new model and how it compares to existing models, is available on GitHub in the form of an R package, see Meijer (2022). An online version of the app can be found on https://gjmeijer.shinyapps.io/DRAM/

List of symbols

All parameters in this manuscript, unless otherwise specified, are expressed in generic dimensions: [F] for units of force, [L] for units of length/diameter, [°] for units of angles and [−] for dimenionsless parameters. This allows the reader to use their own preferred set of units in each equation.

- α: Azimuth angle of displaced root orientation [°]
- α_0: Azimuth angle of undisplaced root orientation [°]
- β: Elevation angle of displaced root orientation [°]
- β_0: Elevation angle of displaced root orientation [°]
- β_F: Fibre bundle model load sharing parameter [−]
- Δx^*: Normalised root displacement in the RBMw by Schwarz et al. (2013) [LL^{-1}]
- ε_r: Root tensile strain [LL^{-1}]
- $\varepsilon_{r,u}$: Root tensile strain at root failure [LL^{-1}]
- $\varepsilon_{r,u,0}$: Root tensile strain at root failure in a root with diameter $d_r = d_{r,0}$ [LL^{-1}]
- $\varepsilon_{r,y}$: Root tensile strain at yielding [LL^{-1}]
- ζ: Intermediate parameter in root stress calculations: $\zeta = t_{r,y}(E_{r,p}^{-1} - E_{r,e}^{-1})$ [−]
- κ: Weibull shape parameter in RBMw model [−]
- κ_t: Weibull shape parameter for (normalised) root tensile strength distribution [−]
- λ: Weibull scale parameter [FL^{-2}]
- λ^*: Weibull scale parameter in the original formulation of RBMw by Schwarz et al. (2013) [−]
- ξ_0: scalar coefficient for constant terms in equation
- ξ_1: scalar coefficient for linear terms in equation
- ξ_2: scalar coefficient for quadratic terms in equation
- ξ_3: scalar coefficient for cubic terms in equation
- ξ_x: Change in root x-coordinate across the shear zone [L]
- ξ_y: Change in root y-coordinate across the shear zone [L]
- σ_n': Normal effective soil stress acting on the shear plane [FL^{-2}]
- τ_i: Root–soil interface shear resistance [FL^{-2}]
- $\tau_{s,u}$: Soil shear strength [FL^{-2}]
- $\tau_{s,r}$: Shear stress applied by roots on soil (just) outside the shear zone [FL^{-2}]
- ϕ': Soil angle of internal friction [°]
- ϕ_r: Root area ratio [L^2L^{-2}]
- A_r: Root cross-sectional area [L^2]
- C_r: Root circumference [L]
- c': Soil (apparent) cohesion [FL^{-2}]
- c_r: (Current) root reinforcement [FL^{-2}]
- $c_{r,u}$: Peak root reinforcement [FL^{-2}]
- d_r: Root diameter [L]
- $d_{r,0}$: Reference diameter [L]
- $E_{r,e}$: Root elastic stiffness [FL^{-2}]
- $E_{r,p}$: Root plastic stiffness [FL^{-2}]
- F: Root tensile force [F]
- f_b: Root breakage parameter [−]
- h: (Current) soil shear zone thickness [L]
- h_0: Initial soil shear zone thickness [L]
- h_{max}: Maximum soil shear zone thickness [L]
- k': Wu/Waldron coefficient [−]
- k'': Sequential mobilisation reduction factor [−]
- L_e: Length of section of root experiencing elastic stresses [L]
- L_p: Length of section of root experiencing plastic stresses [L]
- L_r: Root length [L]
- L_s: Length of root section currently within the shear zone [L]
- s: Coordinate along root axis [L]
- t_r: Root tensile stress [FL^{-2}]
- $t_{r,u}$: Root tensile strength [FL^{-2}]
- $t_{r,u,0}$: Root tensile strength in a root with diameter $d_r = d_{r,0}$ [FL^{-2}]
- $t_{r,y}$: Root tensile stress at yielding [FL^{-2}]
- $t_{r,a}$: Tensile stress in middle of anchored root [FL^{-2}]
- $t_{r,s}$: Tensile stress in middle of slipping root [FL^{-2}]
- u_r: Root elongation [L]
- u_s: Soil direct shear displacement [L]

Declaration of Competing Interest

The authors declare that they have no known competing financial interests or personal relationships that could have appeared to influence the work reported in this paper.

Acknowledgements

The authors acknowledge helpful discussions from all collaborators, as well as the μVIS X-ray Imaging Centre at the University of Southampton for provision of tomographic imaging facilities.

References

Abernethy, B., Rutherfurd, I.D., 2001. The distribution and strength of riparian tree roots in relation to riverbank reinforcement. Hydrol. Proc. 15 (1), 63–79. https://doi.org/10.1002/hyp.152.

Briggs, K.M., Smethurst, J.A., Powrie, W., O'Brien, A.S., 2016. The influence of tree root water uptake on the long term hydrology of a clay fill railway embankment. Transport. Geotech. 9, 31–48. https://doi.org/10.1016/j.trgeo.2016.06.001.

Bull, D.J., Smethurst, J.A., Sinclair, I., Pierron, F., Roose, T., Powrie, W., Bengough, A.G., 2020. Mechanisms of root reinforcement in soils: an experimental methodology using four-dimensional x-ray computed tomography and digital volume correlation. Proceed. Royal Soc. A: Math. Phys. Eng. Sci. 476 (2237), 20190838. https://doi.org/10.1098/rspa.2019.0838.

Bull, D.J., Smethurst, J.A., Meijer, G.J., Sinclair, I., Pierron, F., Roose, T., Powrie, W., Bengough, A.G., 2021. Modelling of stress transfer in root reinforced soils informed by 4d x-ray computed tomography and digital volume correlation data. Proceed. Royal Soc. A: Math. Phys. Eng. Sci. 478, 20210210 https://doi.org/10.1098/rspa.2021.0210 (in press).

Burroughs, E.R., Thomas, B.R., 1977. Declining Root Strength in Douglas-Fir After Felling as a Factor in Slope Stability, Research Paper INT-190. US Department of Agriculture Forest Service, Ogden, Utah.

Comino, E., Marengo, P., Rolli, V., 2010. Root reinforcement effect of different grass species: a comparison between experimental and models results. Soil Tillage Res. 110 (1), 60–68. https://doi.org/10.1016/j.still.2010.06.006.

Coppin, N., Richards, I., 1990. Use of Vegetation in Civil Engineering, CIRIA Book 10. Butterworths Kent, London (UK).

Dazio, E., Conedera, M., Schwarz, M., 2018. Impact of different chestnut coppice managements on root reinforcement and shallow landslide susceptibility. Forest Ecol. Manag. 417 (7), 63–76. https://doi.org/10.1016/j.foreco.2018.02.031.

Ekanayake, J.C., Marden, M., Watson, A.J., Rowan, D., 1997. Tree roots and slope stability: a comparison between pinus radiata and kanuka. New Zealand J. Forestry Sci. 27 (2), 216–233.

Fan, C.-C., Chen, Y.-W., 2010. The effect of root architecture on the shearing resistance of root-permeated soils. Ecol. Eng. 36 (6), 813–826. https://doi.org/10.1016/j.ecoleng.2010.03.003.

Fan, C.-C., Su, C.-F., 2008. Role of roots in the shear strength of root-reinforced soils with high moisture content. Ecol. Eng. 33 (2), 157–166. https://doi.org/10.1016/j.ecoleng.2008.02.013.

Genet, M., Kokutse, N., Stokes, A., Fourcaud, T., Cai, X., Ji, J., Mickovski, S., 2008. Root reinforcement in plantations of cryptomeria Japonica D. Don: effect of tree age and stand structure on slope stability. Forest Ecol. Manag. 256 (8), 1517–1526. https://doi.org/10.1016/j.foreco.2008.05.050.

Giadrossich, F., Schwarz, M., Cohen, D., Preti, F., Or, D., 2013. Mechanical interactions between neighbouring roots during pullout tests. Plant Soil 367 (1-2), 391–406. https://doi.org/10.1007/s11104-012-1475-1.

Gray, D.H., Ohashi, H., 1983. Mechanics of fiber reinforcement in sand. J. Getech. Eng. 109 (3), 335–353. https://doi.org/10.1061/(asce)0733-9410(1983)109:3(335.

Jewell, R.A., Wroth, C.P., 1987. Direct shear tests on reinforced sand. Géotechnique 37 (1), 53–68. https://doi.org/10.1680/geot.1987.37.1.53.

Ji, J., Mao, Z., Qu, W., Zhang, Z., 2020. Energy-based fibre bundle model algorithms to predict soil reinforcement by roots. Plant Soil 446 (1-2), 307–329. https://doi.org/10.1007/s11104-019-04327-z.

Liang, T., Bengough, A.G., Knappett, J., Muir Wood, D., Loades, K.W., Hallett, P.D., Boldrin, D., Leung, A.K., Meijer, G.J., 2017. Scaling of the reinforcement of soil slopes by living plants in a geotechnical centrifuge. Ecol. Eng. 109, 207–227. https://doi.org/10.1016/j.ecoleng.2017.06.067.

Loades, K.W., Bengough, A.G., Bransby, M.F., Hallett, P.D., 2013. Biomechanics of nodal, seminal and lateral roots of barley: effects of diameter, waterlogging and mechanical impedance. Plant Soil 370 (1), 407–418. https://doi.org/10.1007/s11104-013-1643-y.

Mao, Z., Saint-Andre, L., Genet, M., Mine, F.-X., Jourdan, C., Rey, H., Courbaud, B., Stokes, A., 2012. Engineering ecological protection against landslides in diverse mountain forests: choosing cohesion models. Ecol. Eng. 45, 55–69. https://doi.org/10.1016/j.ecoleng.2011.03.026.

Meijer, G.J., 2021. Generic form of fibre bundle models for soil reinforcement by plant roots. Plant Soil 468, 45–65. https://doi.org/10.1007/s11104-021-05039-z.

Meijer, G.J., Bengough, A.G., Knappett, J.A., Loades, K.W., Nicoll, B.C., 2018. In situ measurement of root-reinforcement using the corkscrew extraction method. Can. Geotech. J. 55 (10), 1372–1390. https://doi.org/10.1139/cgj-2017-0344.

Meijer, G.J., Muir Wood, D., Knappett, J.A., Bengough, A.G., Liang, T., 2019a. Analysis of coupled axial and lateral deformation of roots in soil. Int. J. Numer. Anal. Methods Geomech. 43 (3), 684–707. https://doi.org/10.1002/nag.2880.

Meijer, G.J., Muir Wood, D., Knappett, J.A., Bengough, A.G., Liang, T., 2021. Root reinforcement: continuum framework for constitutive modelling. Géotechnique. https://doi.org/10.1680/jgeot.21.00132 (in press).

Meijer, G.J., 2022. GJMeijer/DRAM: v0.1.1 (v0.1.1). Zenodo. https://doi.org/10.5281/zenodo.6375587 (in press).

Meijer, G.J., Muir Wood, D., Knappett, J.A., Bengough, G., Liang, T., 2019b. Root branching affects the mobilisation of root-reinforcement in direct shear. E3S Web Coferences 92, 12010. https://doi.org/10.1051/e3sconf/20199212010.

Mickovski, S.B., Hallett, P.D., Bransby, M.F., Davies, M.C.R., Sonnenberg, R., Bengough, A.G., 2009. Mechanical reinforcement of soil by willow roots: impacts of root properties and root failure mechanism. Soil Sci. Soc. Am. J. 73 (4), 1276–1285. https://doi.org/10.2136/sssaj2008.0172.

Moos, C., Bebi, P., Graf, F., Mattli, J., Rickli, C., Schwarz, M., 2016. How does forest structure affect root reinforcement and susceptibility to shallow landslides? Earth Surface Proc. Landforms 41 (7), 951–960. https://doi.org/10.1002/esp.3887.

Oda, M., Iwashita, K., 1999. Mechanics of Granular Materials: An Introduction. Balkema, Rotterdam (The Netherlands).

Operstein, V., Frydman, S., 2000. The influence of vegetation on soil strength. Ground Improv. 4, 81–89. https://doi.org/10.1680/grim.2000.4.2.81.

Pollen, N., Simon, A., 2005. Estimating the mechanical effects of riparian vegetation on stream bank stability using a fiber bundle model. Water Resour. Res. 41 (7), W07025. https://doi.org/10.1029/2004WR003801.

Postma, J.A., Kuppe, C., Owen, M.R., Mellor, N., Griffiths, M., Bennett, M.J., Lynch, J.P., Watt, M., 2017. Open sim root: widening the scope and application of root architectural models. New Phytologist 215 (3), 1274–1286. https://doi.org/10.1111/nph.14641.

Preti, F., 2013. Forest protection and protection forest: tree root degradation over hydrological shallow landslides triggering. Ecol. Eng. 61, 633–645. https://doi.org/10.1016/j.ecoleng.2012.11.009.

Core Team, S R, 2013. A Language and Environment for Statistical Computing. R Foundation for792 Statistical Computing, Vienna, Austria. http://www.R-project.org.

Schmidt, K.M., Roering, J.J., Stock, J.D., Dietrich, W.E., Montgomery, D.R., Schaub, T., 2001. The variability of root cohesion as an influence on shallow landslide susceptibility in the Oregon Coast Range. Can. Geotech. J. 38 (5), 995–1024. https://doi.org/10.1139/cgj-38-5-995.

Schwarz, M., Cohen, D., Or, D., 2011. Pullout tests of root analogs and natural root bundles in soil: experiments and modeling. J. Geophys. Res.: Earth Surface 116 (F2), F02007. https://doi.org/10.1029/2010jf001753.

Schwarz, M., Giadrossich, F., Cohen, D., 2013. Modeling root reinforcement using a root-failure weibull survival function. Hydrol. Earth Sys. Sci. 17, 4367–4377. https://doi.org/10.5194/hess-17-4367-2013.

Shewbridge, S.E., Sitar, N., 1989. Deformation characteristics of reinforced sand in direct shear. J. Geotech. Eng. (ASCE) 115 (8), 1134–1147. https://doi.org/10.1061/(ASCE)0733-9410(1989)115:8(1134.

Smit, A.L., Bengough, A.G., Engels, C., van Noordwijk, M., Pellering, S., van de Geijn, S. C., 2000. Root Methods, a Handbook. Springer, Berlin, Heidelberg (Germany). ISBN 978-3-642-08602-1.

Stokes, A., Atger, C., Bengough, A.G., Fourcaud, T., Sidle, R.C., 2009. Desirable plant root traits for protecting natural and engineered slopes against landslides. Plant Soil 324 (1-2), 1–30. https://doi.org/10.1007/s11104-009-0159-y.

Thomas, R.E., Pollen-Bankhead, N., 2010. Modeling root-reinforcement with a fiber-bundle model and Monte Carlo simulation. Ecol. Eng. 36 (1), 47–61. https://doi.org/10.1016/j.ecoleng.2009.09.008.

Utomo, W.H., Dexter, A.R., 1981. Age hardening of agricultural top soils. J. Soil Sci. 32 (3), 335–350. https://doi.org/10.1111/j.1365-2389.1981.tb01710.x.

Waldron, L.J., 1977. Shear resistance of root-permeated homogeneous and stratified soil. Soil Sci. Soc. Am. J. 41 (5), 843–849. https://doi.org/10.2136/sssaj1977.03615995004100050005x.

Waldron, L.J., Dakessian, S., 1981. Soil reinforcement by roots: calculation of increased soil shear resistance from root properties. Soil Sci. 132, 427–435.

Wu, T.H., Watson, A., 1998. In situ shear tests of soil blocks with roots. Can. Geotech. J. 35 (4), 579–590. https://doi.org/10.1139/cgj-35-4-579.

Wu, T.H., McKinnell III, W.P., Swanston, D.N., 1979. Strength of tree roots and landslides on Prince of Wales Island. Alaska. Can. Geotech. J. 16 (1), 19–33. https://doi.org/10.1139/t79-003.

Wu, T.H., McOmber, R.M., Erb, R.T., Beal, P.E., 1988. Study of soil-root interaction. J. Geotech. Eng. (ASCE) 114 (12), 1351–1375. https://doi.org/10.1061/(ASCE)0733-9410(1988)114:12(1351.

Zhu, J., Wang, Y., Wang, Y., Mao, Z., Langendoen, E.J., 2020. How does root biodegradation after plant felling change root reinforcement to soil? Plant Soil 446 (1-2), 211–227. https://doi.org/10.1007/s11104-019-04345-x.